Chapter-3

A mechanistic study on solar energized degradation of herbicide into value-added product using -SO_3H functionalized ionic liquid-polyoxometalate based heterogeneous catalyst in aqueous medium

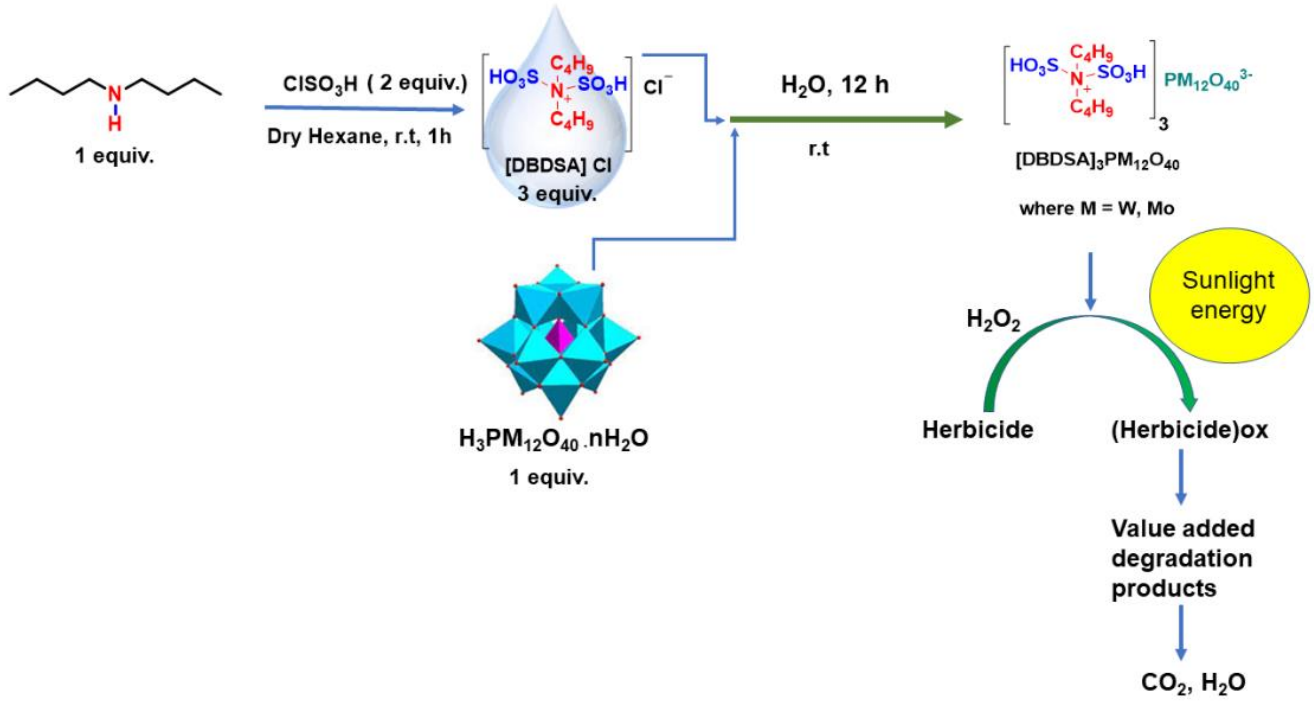

Synopsis: Incorporation of the -SO_3H group into the ammonium-based cation along with hydrophobic dibutyl groups was responsible for the preservation of heterogeneity of the hybrids throughout the reaction in aqueous medium. The recyclable IL-POM hybrids as heterogenous metobromuron degradation catalysts using H_2O_2 as oxidant removed greater than 70% of TOC under sunlight in 8 hours. 1-Bromo-4-isocyanatobenzene yielded as the major value-added product that can be used to synthesize various unsymmetrical disubstituted urea derivatives.

3.1. Introduction

Water reservoir contamination with organic toxic pollutants like pesticides, dyes, etc. is an increasing environmental concern and pollutant degradation and removal is another commonly experienced challenge [1]. Carrying on with the global call on food demand, a broad class of pesticides, namely herbicides, are used to keep up with the requirement so that the growth and yield of desired crops are not compromised. Phenylurea, especially are a prominent group of herbicides used to control weeds as they act as photosynthetic electron transport inhibitors upon photosystem II [2]. Metobromuron (MB) is one among many other types of phenylurea herbicides that are used for the same. Their low absorption in soil and high water solubility lead to contamination of the aquatic reservoirs, deteriorating the quality of water [3,4].

Many treatment techniques like chemical, electrochemical and photochemical processes have been proposed and performed for the removal of organic pollutants from water sources. Those include incineration [5], adsorption on granulated activated carbon [6], air stripping [7] and advanced oxidation processes (AOPs) [8]. According to numerous literature surveys, advanced oxidation processes (AOPs) are observed to have enormous potential to lower the impact of organic pollutants in the environment because of their efficiency in total mineralization and transformation to less harmful degradation products via the formation of reactive oxygen species [8,9]. Fenton, photo-Fenton, O_3/UV, H_2O_2/UV, H_2O_2/O_3/UV, homogeneous as well as heterogeneous photocatalysis using semiconductor catalysts are various methods that have been already used for water treatment [10-14]. Polyoxometalates (POMs) in recent decades are another important

class of redox material used for the development of AOPs, which provide excellent results for oxidation of toxic pollutants for water remediation, in the presence of light [15-18]. Research work on this kind of metal-oxides is expanding in the fields of chemistry, biology, catalysis, molecular electronics, and material science on account of its distinctive properties like strong acidity and redox properties [18,19,20].

POMs outshine as a group of metal oxides and are widely studied due to their structure stability and effectiveness [21]. Investigation into this early transition metal–oxygen clusters with distinctive structural characteristics as efficient multiple functional catalysts is extensively done and still ongoing. A variety of POMs with their transition metal substituted derivatives are said to be multi-electron "reversible" redox catalysts as they can accept and release a certain number of electrons while retaining their structures [22]. POMs adopt d^0 electronic configuration in its fully oxidized state and display intramolecular ligand to metal charge transfer (LMCT) upon irradiation with UV and/or near UV light thus rendering POMs to be strong oxidizing reagents with oxidation of the organic compounds present as substrates [23,24]. TiO_2 is another extensively used metal oxide catalyst for oxidation of organic pollutants. Even though POMs being less toxic compared to TiO_2 and display similar catalytic activities like TiO_2, they are paid less recognition [25,26,27]. The reason behind this is POM's strong Brönsted acidic property which makes them soluble in aqueous medium, polar solvents and makes its recovery laborious from the reaction system for recyclability [28].

Considering, both the advantages and disadvantages of POMs, there is a need to develop a type of POM-based catalytic system with more advantages, which will be a recoverable one and water tolerant in nature to carry out degradation of contaminants in aqueous medium [27]. Various attempts by research groups have been made to design modified POM systems that enhance the catalytic activity of the POM-based catalysts besides their easy recovery. Considering their high solubility in aqueous medium and polar solvents, methods like immobilization of POMs on active carbon and carbon fibers, impregnation of POMs on TiO_2 or silica gels, intercalation of POMs into anionic clays, and combination of POMs with suitable counterions have been practiced [29]. Numerous ionic liquids with different structures have already been used as a suitable counterion for synthesizing various organic-inorganic hybrids. Ionic liquids are well known for having melting points below 100 ºC with extremely low vapor pressure and can be tuned into functionalized ion pairs as desired [30, 31].

In this report, to resolve the high solubility issue of POMs and to extend their usage as suitable oxidative catalyst, POMs were incorporated into -SO_3H functionalized chloride-based ionic liquid via anion exchange leading to IL-POM hybrid. Synthesized hybrids display selective solubility in various solvents and more importantly are water-insoluble and can be used as recyclable heterogeneous catalysts for oxidative degradation of pollutants in aqueous medium. Integration of -SO_3H functionalized dialkylammonium based IL consisting of two hydrophobic n-butyl groups with classical Keggin POMs allowed extensive hydrogen bonding of the organic cation with the inorganic anion hence modifying both physical/chemical properties, particularly highlighting its application for herbicide degradation in aqueous medium.

Thus, it is possible to achieve miscellaneous new compounds with enhanced features by tailoring the organic ionic liquid cation with various functional groups according to the need of its application [32]. The synthesized IL-POMs were used as oxidative catalysts with H_2O_2 as a mild oxidant for herbicide degradation in aqueous medium both in the presence and absence of sunlight.

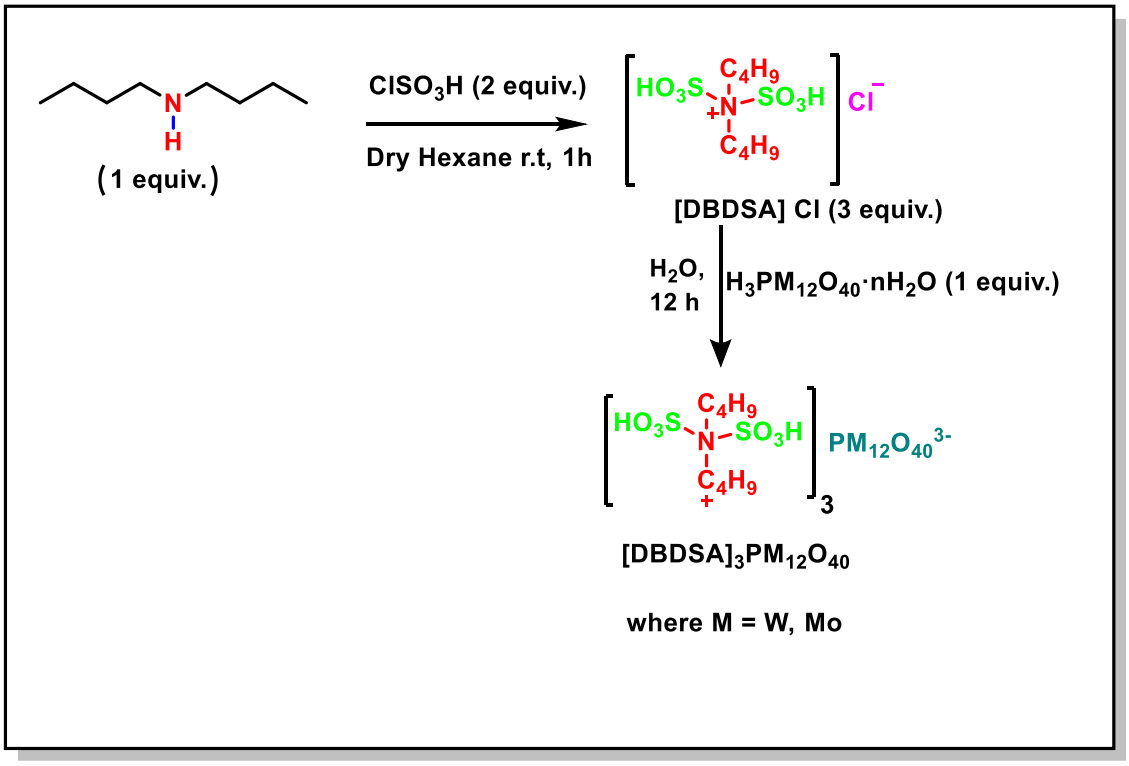

Scheme 3.1: Synthesis of $[DBDSA]_3PM_{12}O_{40}$ hybrid salt material.

3.2. Results and discussion

The preparation of polyoxometalate hybrid salts $[DBDSA]_3PM_{12}O_{40}$ of dibutyl disulfoammonium cation $[DBDSA]^+$ in combination with $[PM_{12}O_{40}]^{3-}$ as counterion, where M= Mo & W were carried out as solid hydrophobic material in water after reaction of 1 equivalent of $H_3PMo_{12}O_{40}\cdot nH_2O$ or $H_3PW_{12}O_{40}\cdot nH_2O$ with 3 equivalents of dibutyl disulfoammonium chloride [DBDSA]Cl as the precursor ionic liquid (**Scheme 3.1**). This is an anion exchange reaction in which 3 protons of the heteropoly acids were exchanged with the organic cations of ionic liquids that led to the IL-POM hybrids with various secondary interactions like H-bonding and ion-dipole interactions resulted in modification of the physical state of the polyoxometalate anions within the hybrids.The characterization of ionic liquid-polyoxometalate hybrids were done by different analytical techniques like FT-IR, ^{1}H NMR, ^{13}C NMR,^{31}P NMR, CHN, TGA, PXRD, Raman, SEM-EDX etc.

3.2.1 FT-IR analysis

The characteristic FT-IR peaks of the [DBDSA]Cl ionic liquid, heteropolyacids $H_3PMo_{12}O_{40}\cdot nH_2O$ and $H_3PW_{12}O_{40}\cdot nH_2O$ along with the IL-POM hybrids $[DBDSA]_3[PMo_{12}O_{40}]$ and $[DBDSA]_3[PW_{12}O_{40}]$ are depicted in **Fig. 3.1**. The typical FT-IR bands of heteropoly anions are seen to retain their fingerprint bands in the hybrids as well at 1065, 956, 870 and 790 cm^{-1} [33]. The medium intensity peak at 1628 cm^{-1} of the parent IL expresses bending vibration of absorbed water molecules. The same frequency at 1628 cm^{-1} of heteropolyacids can also be allocated to bending vibration of water molecules present in secondary structures of the Keggin anions. Noteworthy that the peak at 1628 cm^{-1} found in both the parent compounds is shifted to 1595 cm^{-1} in the case of the hybrids. This may have happened because of the loss of water molecules from the Keggin anions due to incorporation of organic cation from ionic liquid into polyoxometalate anion".

The asymmetric and symmetric S-O stretches of sulfonic groups are observed around 1229 and 1165 cm^{-1} respectively. The N-S stretching vibration has been observed to overlap with the characteristic asymmetric P-O stretch of the polyoxometalate unit in the range of 847-879 cm^{-1}. Peaks observed at 2869, 2935, 2960, 3192 cm^{-1} are assigned to aliphatic C-H stretches of two butyl groups bind to the nitrogen. They also showed C-H

rocking at 1377 cm^{-1} and C-H bending at 1455 cm^{-1} in the respective IR spectra of the IL-POMs.

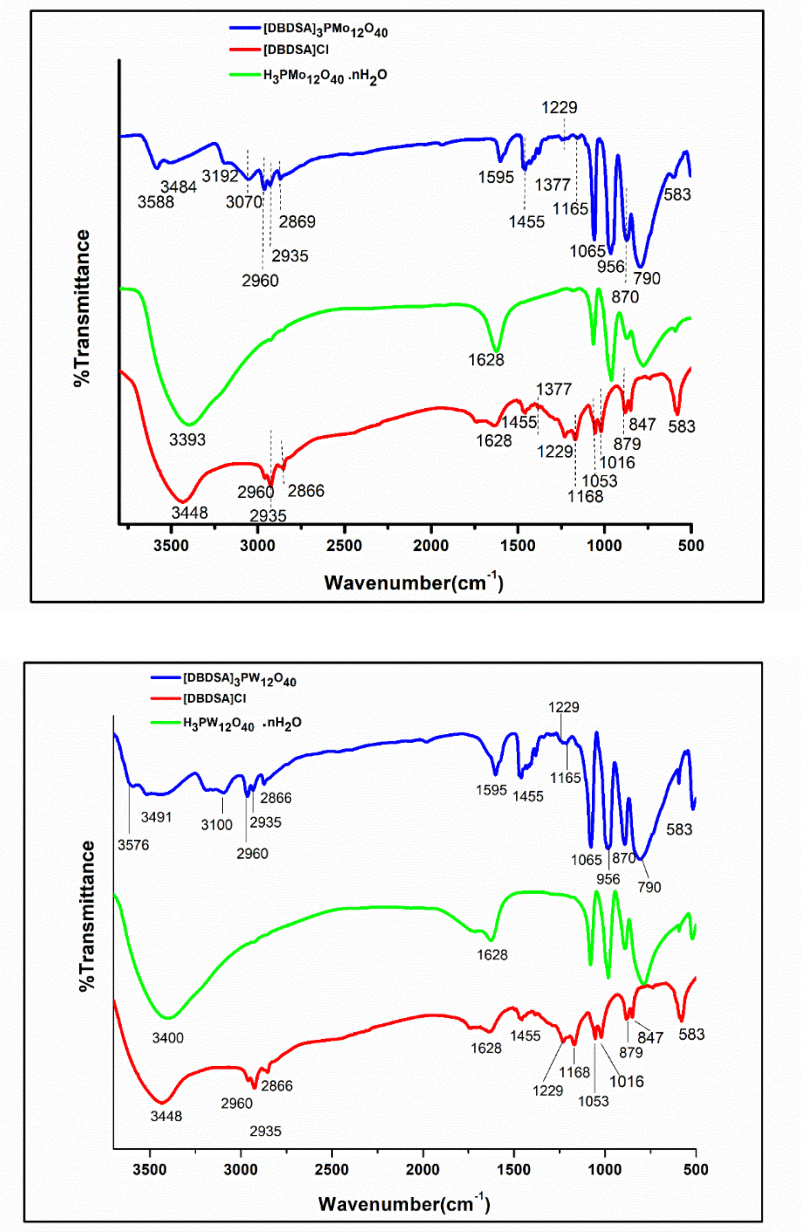

Fig. 3.1: FT-IR spectra of (a) $H_3PMo_{12}O_{40}\cdot nH_2O$, [DBDSA]Cl and $[DBDSA]_3[PMo_{12}O_{40}]$ (b) $H_3PW_{12}O_{40}\cdot nH_2O$, [DBDSA]Cl and $[DBDSA]_3[PW_{12}O_{40}]$ respectively.

The O-H stretch of IL-POM hybrid of $[PMo_{12}O_{40}]^{3-}$ displayed two medium intensity peaks at 3484 and 3588 cm^{-1} which can be attributed to O-H bond of the sulfonic groups and H-bonded water molecules with the Keggin anion. Likewise, the O-H stretch of $[PW_{12}O_{40}]^{3-}$ hybrid showed medium intensity vibrations at 3491 cm^{-1} and 3576 cm^{-1} against the O-H peaks of chloride IL at 3448 cm^{-1}, 3393 cm^{-1} for the phosphomolybdic

acid and 3400 cm^{-1} for the phosphotungstic acid respectively. The reduction of the peak intensity of O-H peaks in the hybrids indicates a decreasing amount of water molecules in the rigid framework of the phosphomolybdate anion and phosphotungstate anion [34].

3.2.2 NMR analysis

The NMR (^{1}H &^{13}C) of [DBDSA]Cl (**Fig. 3.2**) and (^{1}H, ^{13}C and ^{31}P) of the $[DBDSA]_3[PMo_{12}O_{40}]$ and $[DBDSA]_3[PW_{12}O_{40}]$ hybrids in DMSO-d_6 are presented in below as (**Fig. 3.3 & 3.4**). The ^{1}H NMR spectrum of phosphomolybdate hybrid showed two $–CH_3$ groups as triplet at 0.86 ppm, sextet for $-CH_2$ group at 1.30 ppm and quintet at 1.50 ppm for adjacent $-CH_2$ group. A triplet at 2.84 ppm is assigned to the $-CH_2$ group adjacent to nitrogen atom of dibutylamine cation. A two-proton singlet is observed for the two $–SO_3H$ protons at 8.14 ppm in **Fig. 3.3** (**a**). Similar peaks for ^{1}H NMR of dibutylamine cation for $[DBDSA]_3PW_{12}O_{40}$ were also observed in **Fig. 3.3** (**c**) with assignment of two $–CH_3$ groups as triplet at 0.86 ppm, two $-CH_2$ group as sextet at 1.30 ppm, two adjacent $-CH_2$ group as quintet at 1.50 ppm and also the $-CH_2$ group as triplet at 2.84 ppm nearer to nitrogen of the dibutylamine cation. The ^{13}C NMR of these IL-POM hybrids displayed four peaks at 14.01, 19.77, 28.09 and 47.09 ppm for $[DBDSA]_3[PMo_{12}O_{40}]$ and 14.02, 19.77, 28.09 and 47.07 ppm for $[DBDSA]_3PW_{12}O_{40}$ hybrid, **Fig. 3.3** (**b**) and **Fig. 3.3** (**d**) respectively. The ^{31}P NMR spectrum of the pure phosphomolybdic acid is found at -3.50 ppm, **Fig. 3.4** (**c**) which almost coincides with the $[DBDSA]_3[PMo_{12}O_{40}]$ hybrid salt, Fig. **3.4** (**a**). A kind of frequency shift of the hybrid in $[DBDSA]_3PW_{12}O_{40}$ is also observed at -15.0 ppm (**Fig. 3.4 b**) compared to a single peak at -14.72 ppm for the pure phosphotungstic acid (**Fig. 3.4 d**). The shifting of peaks in ^{31}P NMR towards lower frequency depicts the loss of physisorbed water during the formation of POM-IL hybrids by the pairing of organic cation and polyoxometalate anion [35].

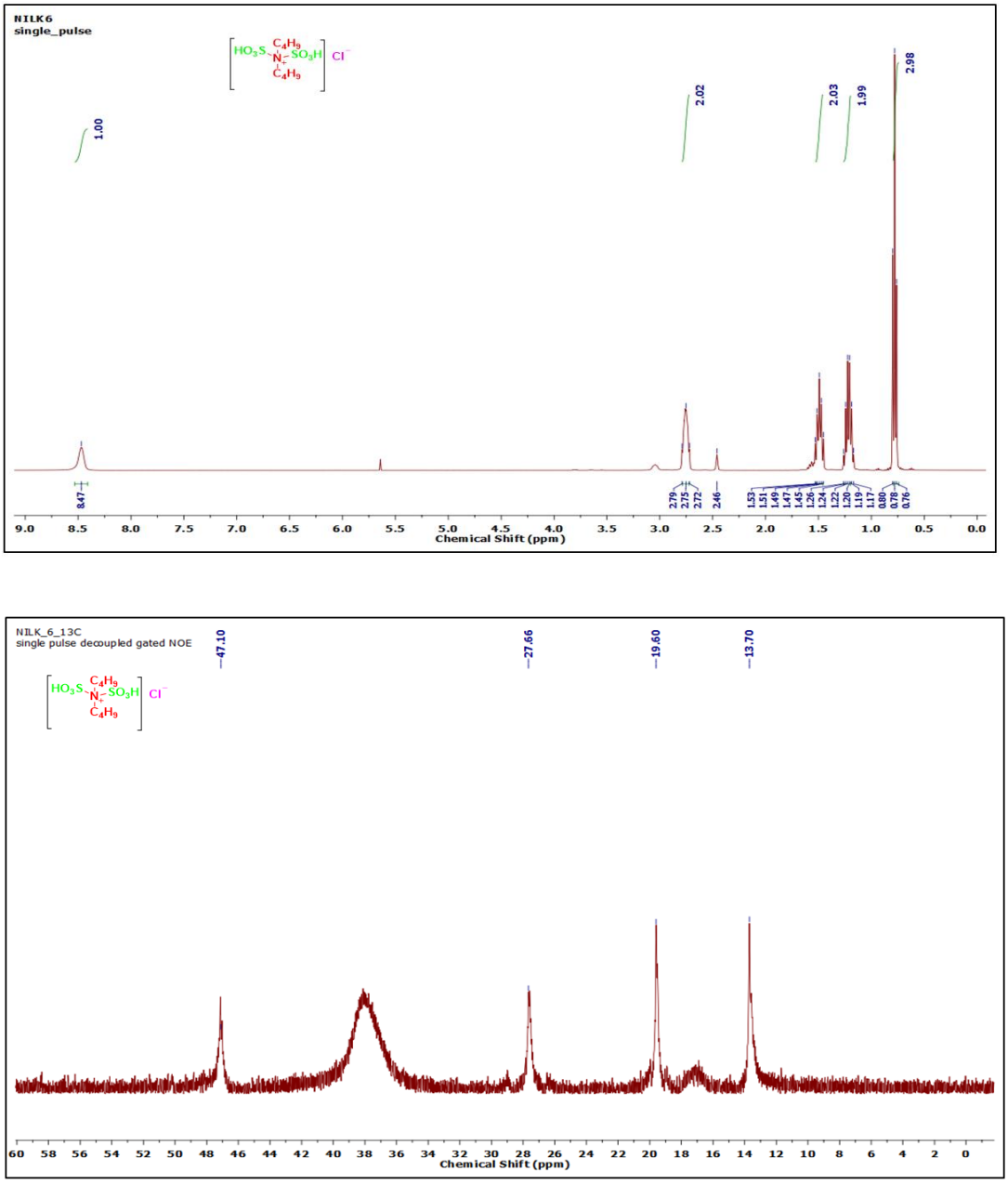

Fig. 3.2: (**a**) ^{1}H NMR spectrum of [DBDSA]Cl and (**b**) ^{13}C NMR spectrum of [DBDSA]Cl.

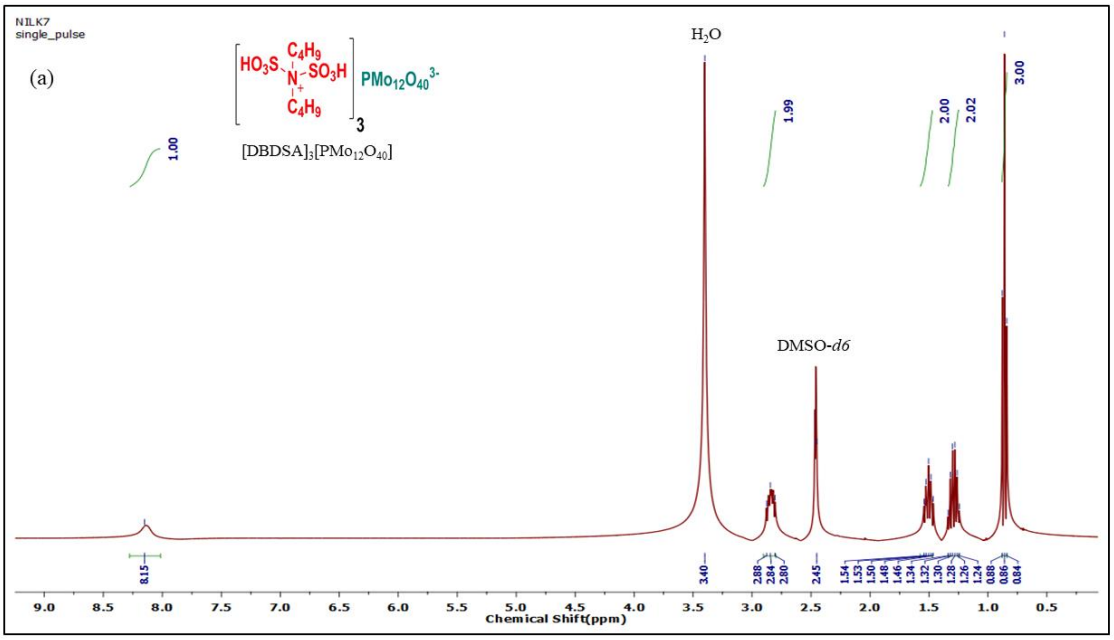
NILK7
single_pulse
(a)
HO_3S C_4H_9 SO_3H C_4H_9 $PMo_{12}O_{40}^{3-}$ 3
$[DBDSA]_3[PMo_{12}O_{40}]$
H_2O
DMSO-*dδ*
1.00
1.99
2.00
2.02
3.00
8.15
3.40
2.88
2.84
2.80
2.45
1.54
1.53
1.50
1.48
1.46
1.34
1.32
1.30
1.28
1.26
1.24
0.88
0.86
0.84
9.0 8.5 8.0 7.5 7.0 6.5 6.0 5.5 5.0 4.5 4.0 3.5 3.0 2.5 2.0 1.5 1.0 0.5
Chemical Shift(ppm)

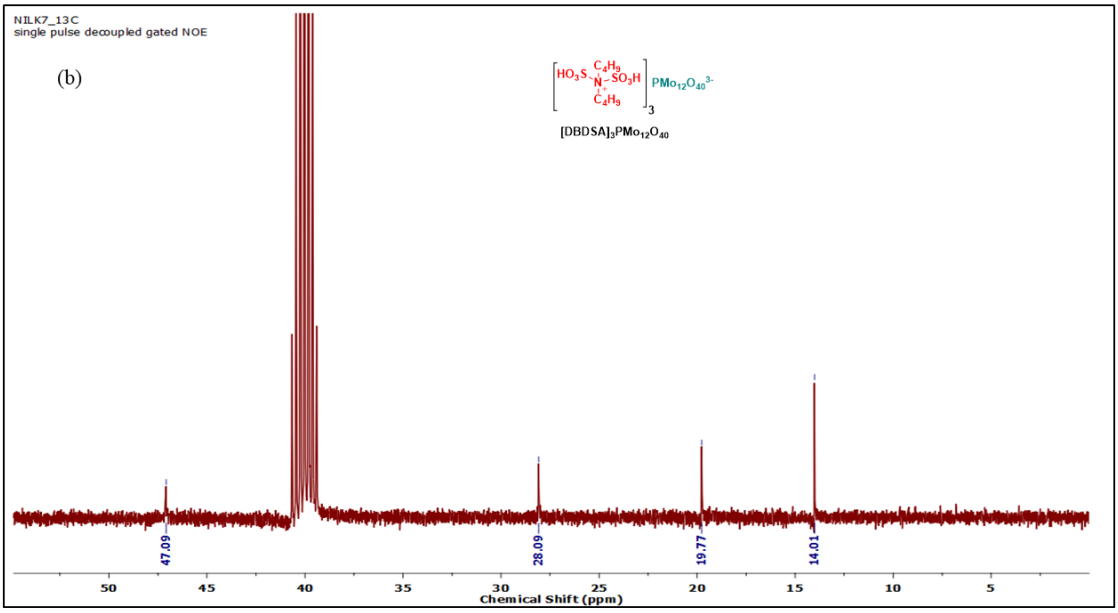
NILK7_13C
single pulse decoupled gated NOE
(b)
HO_3S C_4H_9 SO_3H C_4H_9 $PMo_{12}O_{40}^{3-}$ 3
$[DBDSA]_3PMo_{12}O_{40}$
47.09
28.09
19.77
14.01
50 45 40 35 30 25 20 15 10 5
Chemical Shift (ppm)

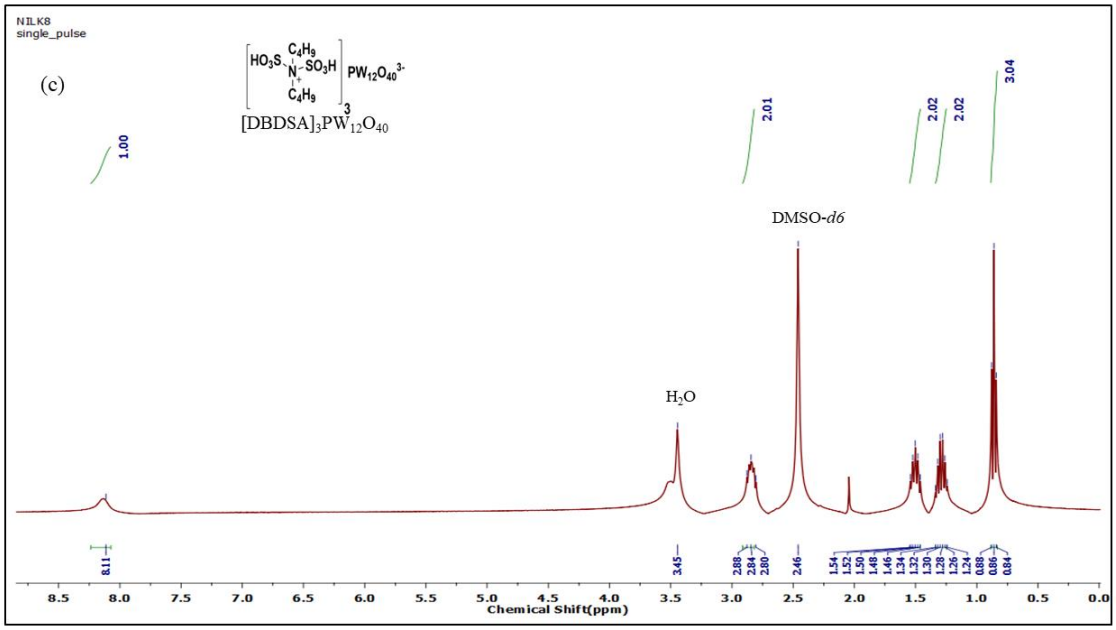

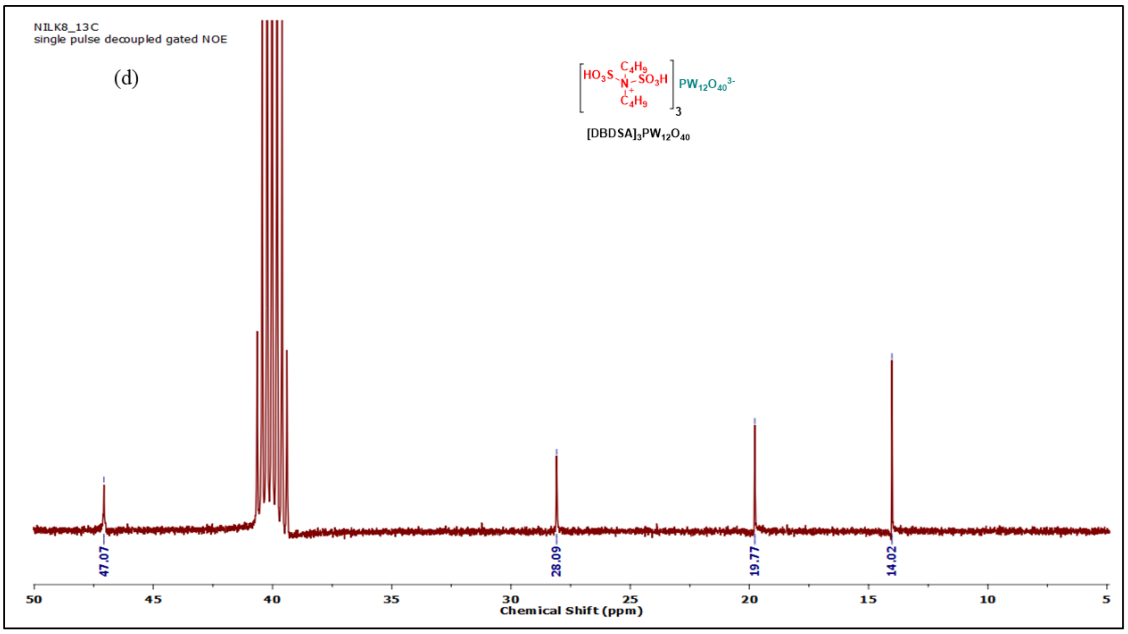

Fig 3.3: ^{1}H NMR spectra of (**a**) ^{1}H NMR of [DBDSA]$_3$[PMo$_{12}$O$_{40}$], (**b**) ^{13}C NMR spectra of [DBDSA]$_3$[PMo$_{12}$O$_{40}$], (**c**) ^{1}H NMR of [DBDSA]$_3$[PW$_{12}$O$_{40}$], (**d**) ^{13}C NMR spectra of [DBDSA]$_3$[PW$_{12}$O$_{40}$].

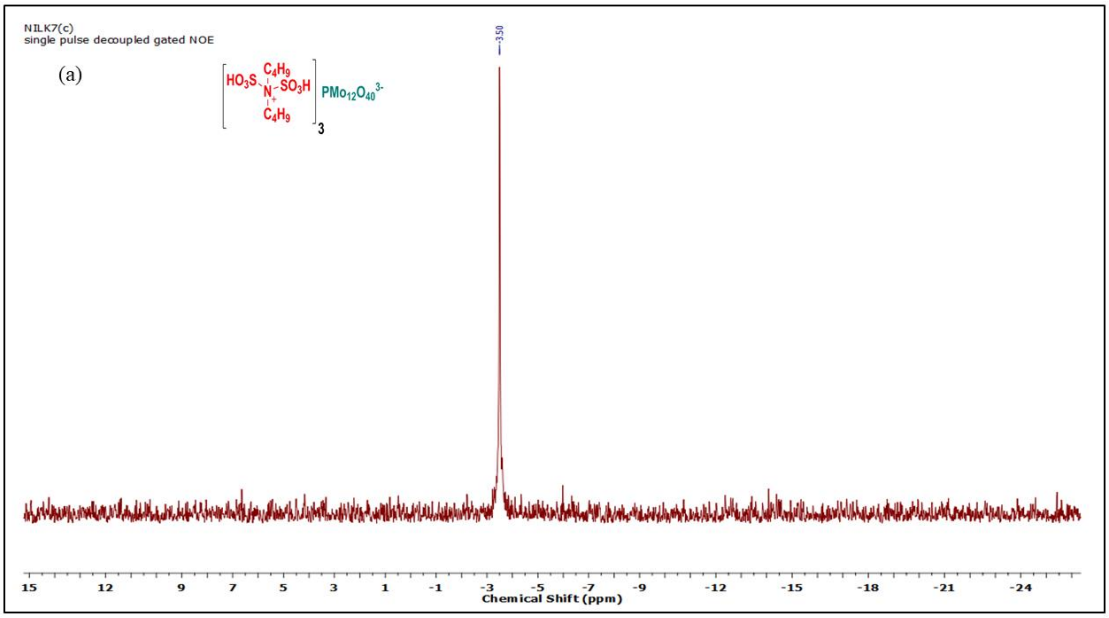
NILK7(c)
single pulse decoupled gated NOE
(a)
$[HO_3S{-}N^{+}(C_4H_9)_3{-}SO_3H]_3\,PMo_{12}O_{40}^{3-}$
-3.50
15 12 9 7 5 3 1 -1 -3 -5 -7 -9 -12 -15 -18 -21 -24
Chemical Shift (ppm)

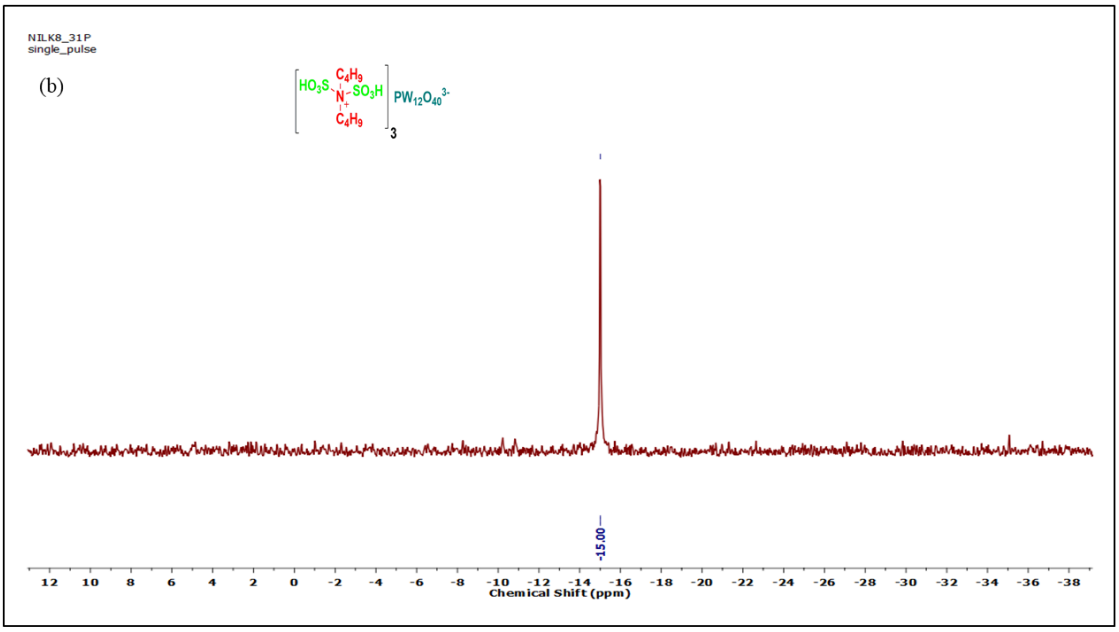
NILK8_31P
single_pulse
(b)
$[HO_3S{-}N^{+}(C_4H_9)_3{-}SO_3H]_3\,PW_{12}O_{40}^{3-}$
-15.00
12 10 8 6 4 2 0 -2 -4 -6 -8 -10 -12 -14 -16 -18 -20 -22 -24 -26 -28 -30 -32 -34 -36 -38
Chemical Shift (ppm)

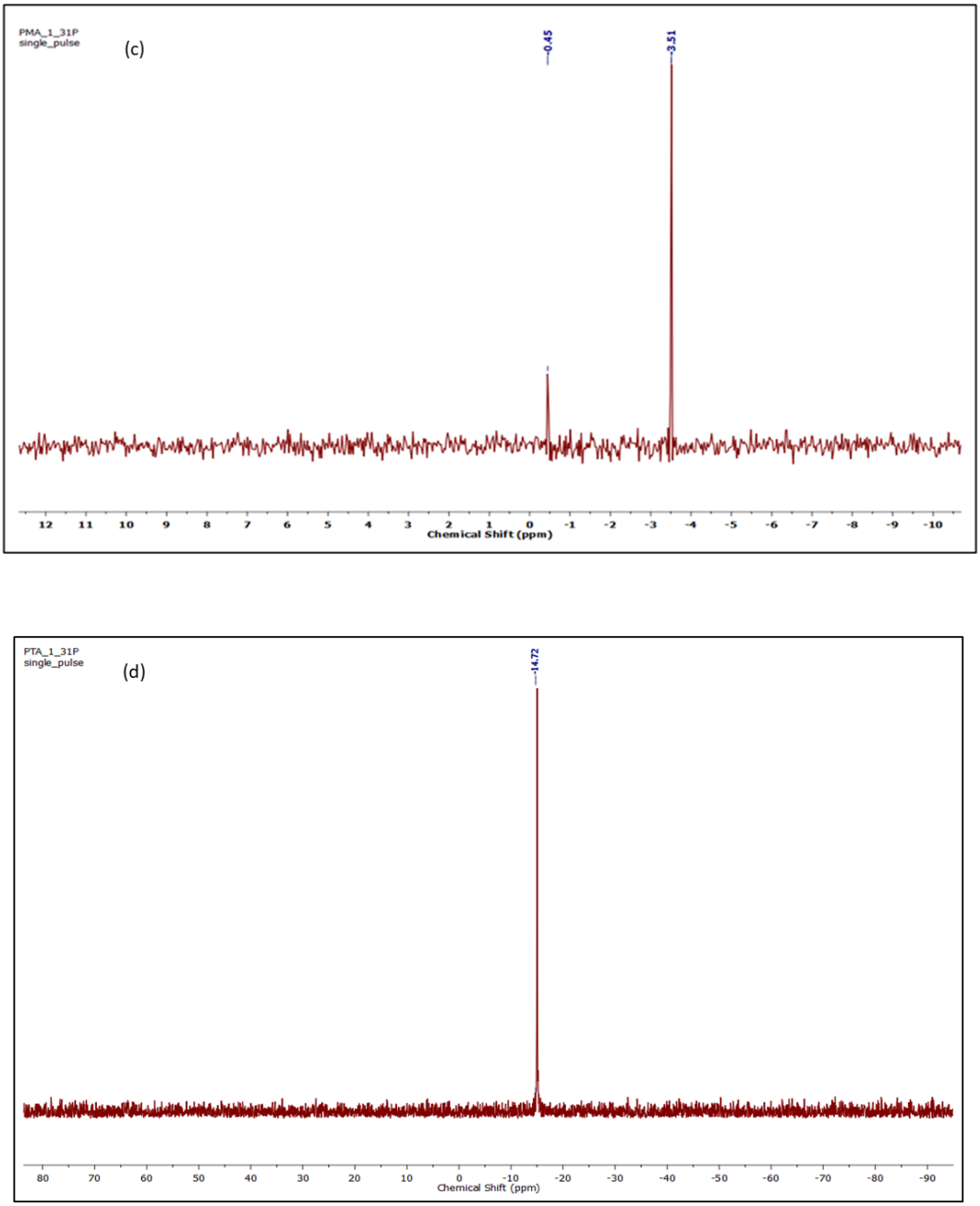

Fig. 3.4: ^{31}P NMR spectra of (**a**) $[DBDSA]_3[PMo_{12}O_{40}]$, (b) $[DBDSA]_3[PW_{12}O_{40}]$, (c) $H_3PMo_{12}O_{40}\cdot nH_2O$ (**d**) $H_3PW_{12}O_{40}\cdot nH_2O$.

3.2.3 Elemental analysis

The CHN analysis results prove that three units of parent ionic liquid cation are bonded against one unit of polyoxometalate anion. Calculated for $[DBDSA]_3PMo_{12}O_{40}$ (%): C 10.60, H 2.20 N 1.54, Found: C 11.01, H 2.15, N 1.56. Calculated for $[DBDSA]_3PW_{12}O_{40}$ (%): C 7.68, H 1.60, N 1.12. Found: C 7.92, H 1.67, N 1.08. For

further structural confirmation, ICP-OES analysis was performed for $[DBDSA]_3[PMo_{12}O_{40}]$ and $[DBDSA]_3[PW_{12}O_{40}]$. The results are tabulated in **Table 3.1.**

Table 3.1: ICP-OES analyses for metal content of the IL-POM hybrids

Entry	Sample	% of metal content Calculated (Found)
1.	$[DBDSA]_3[PMo_{12}O_{40}]$	Mo, 42.6 (43.4 %)
2.	$[DBDSA]_3[PW_{12}O_{40}]$	W, 58.8 (59.4%)

3.2.4 TGA

Thermogravimetric analysis (TGA) displays that as the ionic liquid (IL) is incorporated into POM anions, the physisorbed water is reduced due to incorporation of the bulkier organic cation into the pores of polyoxometalate during the process of metathesis (**Fig. 3.5**). The thermal stability of [DBDSA]Cl ionic liquid observed up to 230 ºC with loss of approximately 24% of physisorbed water at 100 ºC. Both the hybrids did not lose any physisorbed water around 100 ºC as compared to their TGA patterns of respective parent heteropolyacids. Additionally, the reduction of peak intensity for O-H stretch in the FT-IR spectra also supported the depletion of physisorbed water in the POM-IL hybrids. The TGA plot of phosphotungstate hybrid showed higher stability up to 440 ºC in contrast to the stability of phosphomolybdate hybrid till 250 ºC. The strong ionic interaction of the organic cation with the Keggin anion is attributed to lesser decomposition of the hybrid even at higher temperatures [36]. Thus, these hybrids can be effectively used as heterogeneous catalyst without worrying about their decomposition or leaching and their special water-insoluble property makes them efficient catalysts for performing degradation reactions in aqueous media.

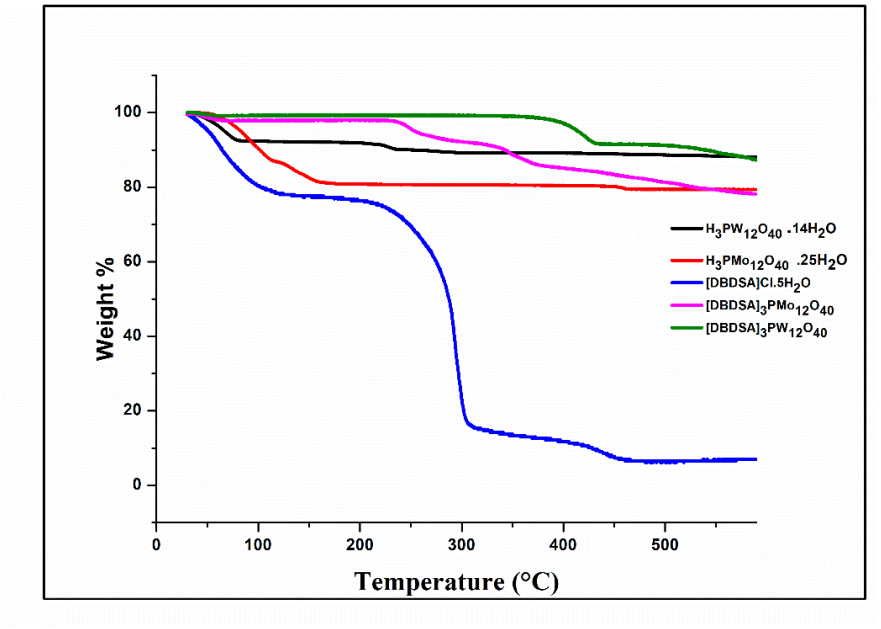

Fig. 3.5: TGA curves of $[DBDSA]_3[PW_{12}O_{40}]$, $[DBDSA]_3[PMo_{12}O_{40}]$, $[DBDSA]Cl{\cdot}5H_2O$, $H_3PMo_{12}O_{40}{\cdot}25H_2O$ and $H_3PW_{12}O_{40}{\cdot}14H_2O$.

3.2.5 Powder XRD analysis

As we compare the Powder-XRD patterns of the heteropolyacids to the synthesized IL-POM hybrids (**Fig. 3.6**), there emerges a lot of changes in the peak intensities. This may have happened due to replacement of dynamic equilibrium acidic protons and the physisorbed water molecules present in the heteropolyacids by bigger sized dibutyldisulfoammonium cations with the reorganization of secondary structures of the polyoxometalates framework. In the hybrids, the bulkier organic cation will be involved in H-bonded interactions *via* two sulfonic groups of OH protons with the Keggin anions instead of the water molecules that were present earlier. In both the hybrids, we can see that in the greater 2Θ region, the Braggs peaks are very weak. The characteristic highly intense peaks of the pure phosphomolybdic acid are retained in the smaller 2Θ region of $[DBDSA]_3[PMo_{12}O_{40}]$. The intensity of the peak at 2Θ= 26.79° has been lowered with the raising of another peak at 24.95° in $[DBDSA]_3[PMo_{12}O_{40}]$ compared to parent phosphomolybdic acid. Again, in $[DBDSA]_3[PW_{12}O_{40}]$, we observe peak at 2Θ= 18.46° has lowered its intensity compared to the parent phosphotungstic acid. The characteristic high intensity peaks in the smaller 2Θ region at 6.79° and 8.55° has shifted its peak position in the respective hybrid. These obvious changes of PXRD patterns in comparison of the parent heteropolyacids with their IL-POM hybrids indicate a reduction

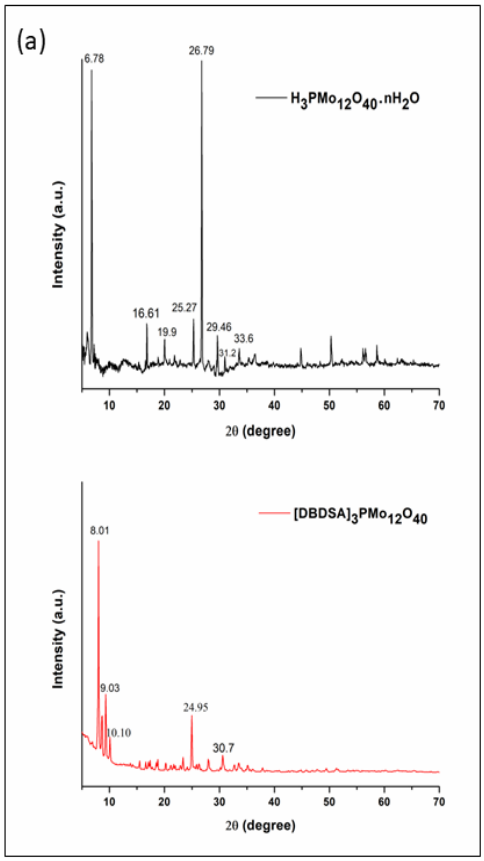

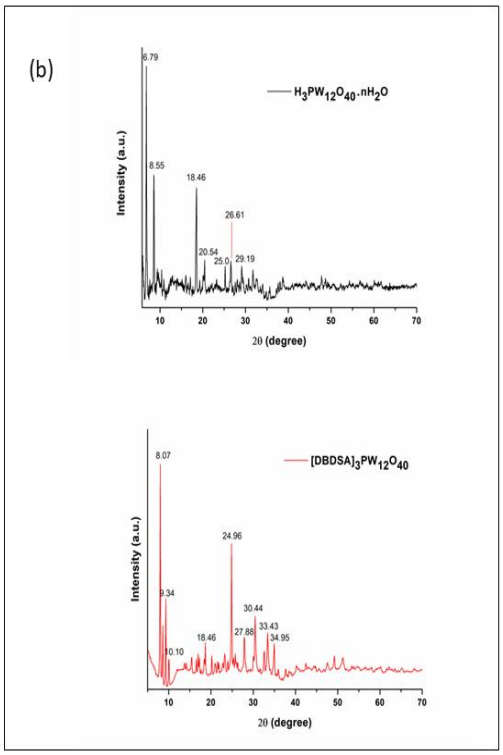

Fig. 3.6: Powder XRD analysis patterns of $H_3PMo_{12}O_{40}\cdot nH_2O$ and $[DBDSA]_3[PMo_{12}O_{40}]$; $H_3PW_{12}O_{40}\cdot nH_2O$ and $[DBDSA]_3[PW_{12}O_{40}]$.

in crystallinity in hybrids and rearrangement in the crystal structure due to electrostatic and H-bonding interactions of the bigger organic cation with the Keggin anions.

3.2.6 Raman analysis

Analysis of Raman spectra of both the hybrids are done as per Bridgeman's assignment [33, 37] of peaks of the respective Keggin anions $[PMo_{12}O_{40}]^{3-}$ and $[PW_{12}O_{40}]^{3-}$ in **Fig. 3.7**. The sharp peak at 991 cm^{-1} for the phosphomolybdate hybrid (**Fig. 3.7a**) is found for symmetric stretch of Mo-O_t. The neighboring less intensity peak at lower frequencies at 890 cm^{-1} is for asymmetric (Mo-O_{2c2}-Mo) bonds. It is well known that the phosphomolybdate is grouped into Mo_3O_{13}, and thus a weak intensity at 610 cm^{-1} is a united band for stretching and bending motion of Mo-O_{2c1}-Mo bonds of the $[Mo_3O_{13}]$ group. The band towards the lowest frequency at 245 cm^{-1} is allocated to the symmetric stretching of Mo-O_{4c} bonds. The $[DBDSA]_3[PW_{12}O_{40}]$ hybrid has almost similar Raman bands, in the **Fig. 3.7** (**b**). Peaks at 1004 cm^{-1} are assigned to symmetric W-O_t and peak at 914 cm^{-1} to asymmetric stretch of W-O_t, asymmetric stretch of W-O_{2c1}-W and asymmetric stretch of W-O_{2c2}-W bond. The combined stretching and bending vibrations of W-O_{2c1}-W in tungstate anion are observed at 528 cm^{-1} in case of the phosphotungstate hybrid. Peak at 228 cm^{-1} is assigned to symmetric stretch of W-O_{4c} bonds.

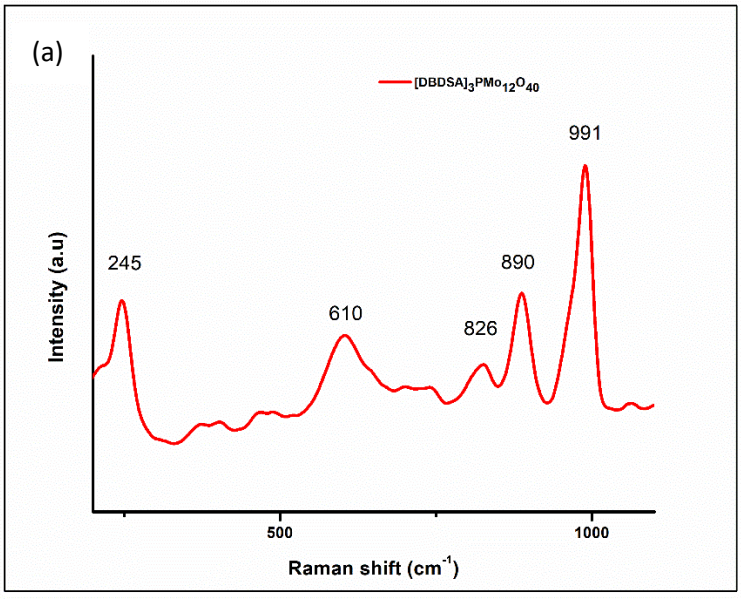

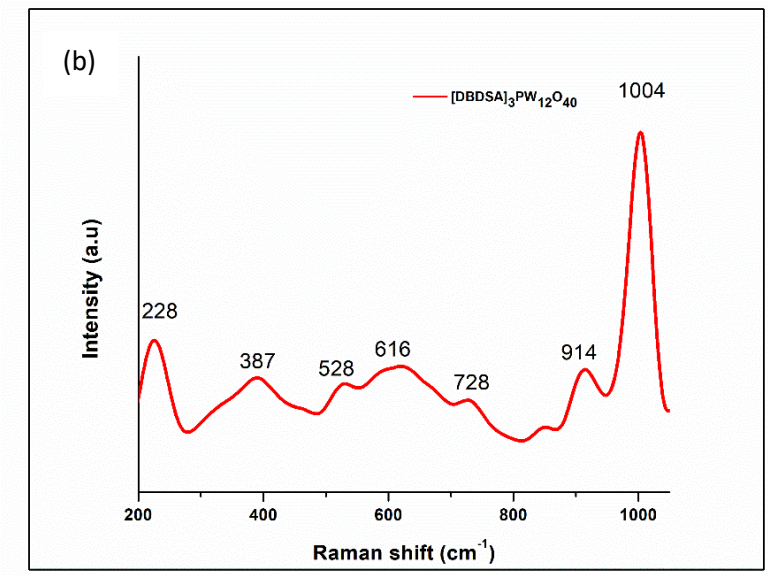

Fig. 3.7: Raman spectra of (**a**) $[DBDSA]_3[PMo_{12}O_{40}]$ and (**b**) $[DBDSA]_3[PW_{12}O_{40}]$.

3.2.7 UV-DRS analysis and Tauc Plots

In **Fig. 3.8**, the diffuse reflectance spectra of pure heteropolyacids vs synthesized IL-POMs displays that the LMCT bands shift towards lower wavelength in hybrid compared to pure heteropolyacids. It is well known that because of the different polarization power of the counter cations, the band shifts towards higher and lower wavelengths accordingly [38]. The results obtained here resonate with the fact that for voluminous counter cation, the band shifts towards a lower wavelength due to decrease in the polarization power of the cation and thus the distance between the heteropolyanions increases. From **Fig. 3.8**, it can be said that the absorbance maxima for the LMCT at 455 nm for phosphomolybdic acid is shifted towards lower wavelength 395 nm in $[DBDSA]_3[PMo_{12}O_{40}]$. Similar results were observed in case of $[DBDSA]_3[PW_{12}O_{40}]$ and phosphotungstic acid. These spectra demonstrate the existence of strong interaction within constituent anion-cation of the IL- POM hybrids and thus reflect the formation of hybrids. **Fig. 3.9** (**a**) and (**b**) are Tauc plots of the IL-POMs. To find the Eg value, graph of $\alpha h\upsilon^2(eV/cm)^2$ vs. Photon energy $h\upsilon$ (eV) is plotted where α is the absorption coefficient, h is the Planck's constant, υ the frequency of vibration, Eg the band gap energy in eV [39]. A straight-line tangent from the curve is drawn. The intersection points of the tangent and the x-axis are the band gap energies. From our spectral analysis, we can interpret that as the ionic liquid is incorporated into the heteropolyanions, the band gap increases [40]. The band gap energy of the hybrids

$[DBDSA]_3PMo_{12}O_{40}$ and $[DBDSA]_3PW_{12}O_{40}$ are found to be 2.50 eV and 3.22 eV respectively.

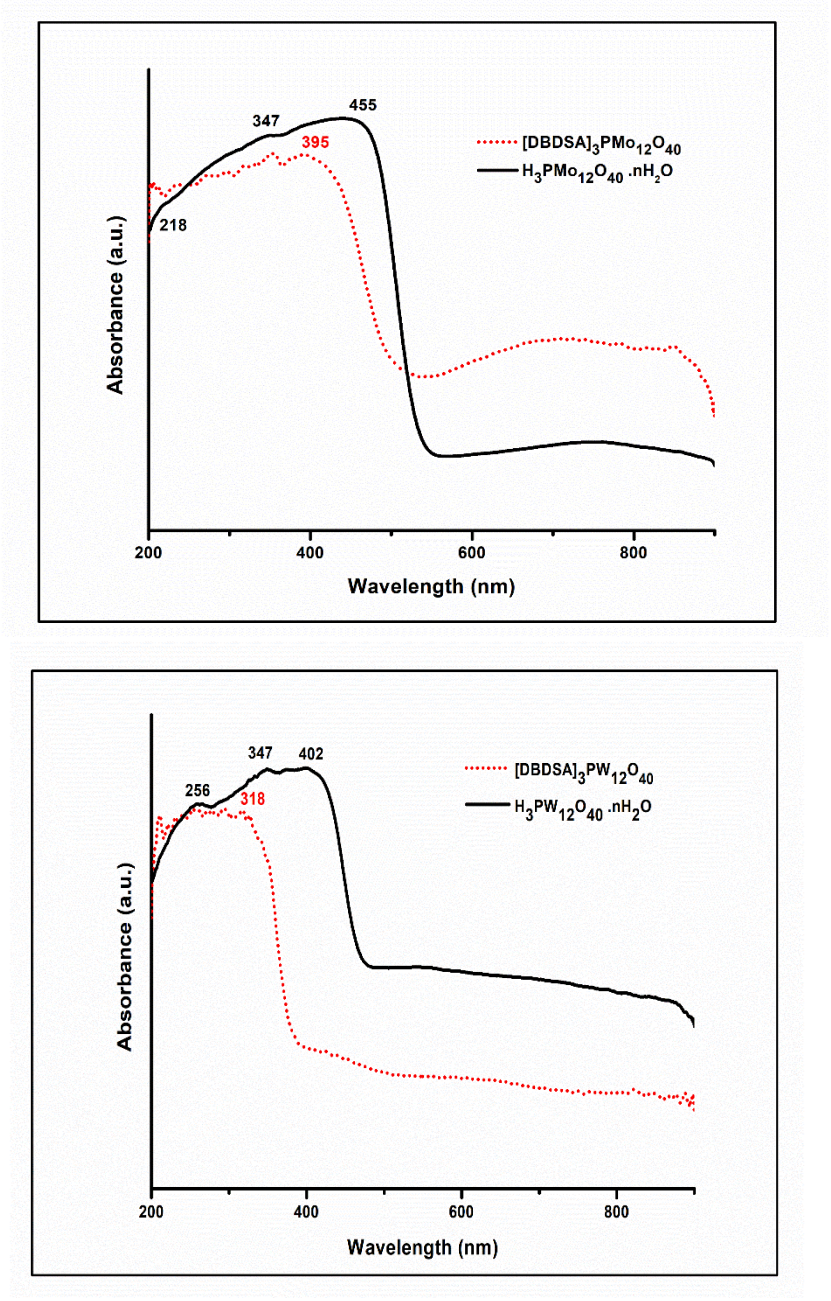

Fig. 3.8: UV–Vis DRS of $[DBDSA]_3[PMo_{12}O_{40}]$ and $H_3PMo_{12}O_{40}\cdot nH_2O$; $[DBDSA]_3[PW_{12}O_{40}]$ and $H_3PW_{12}O_{40}\cdot nH_2O$.

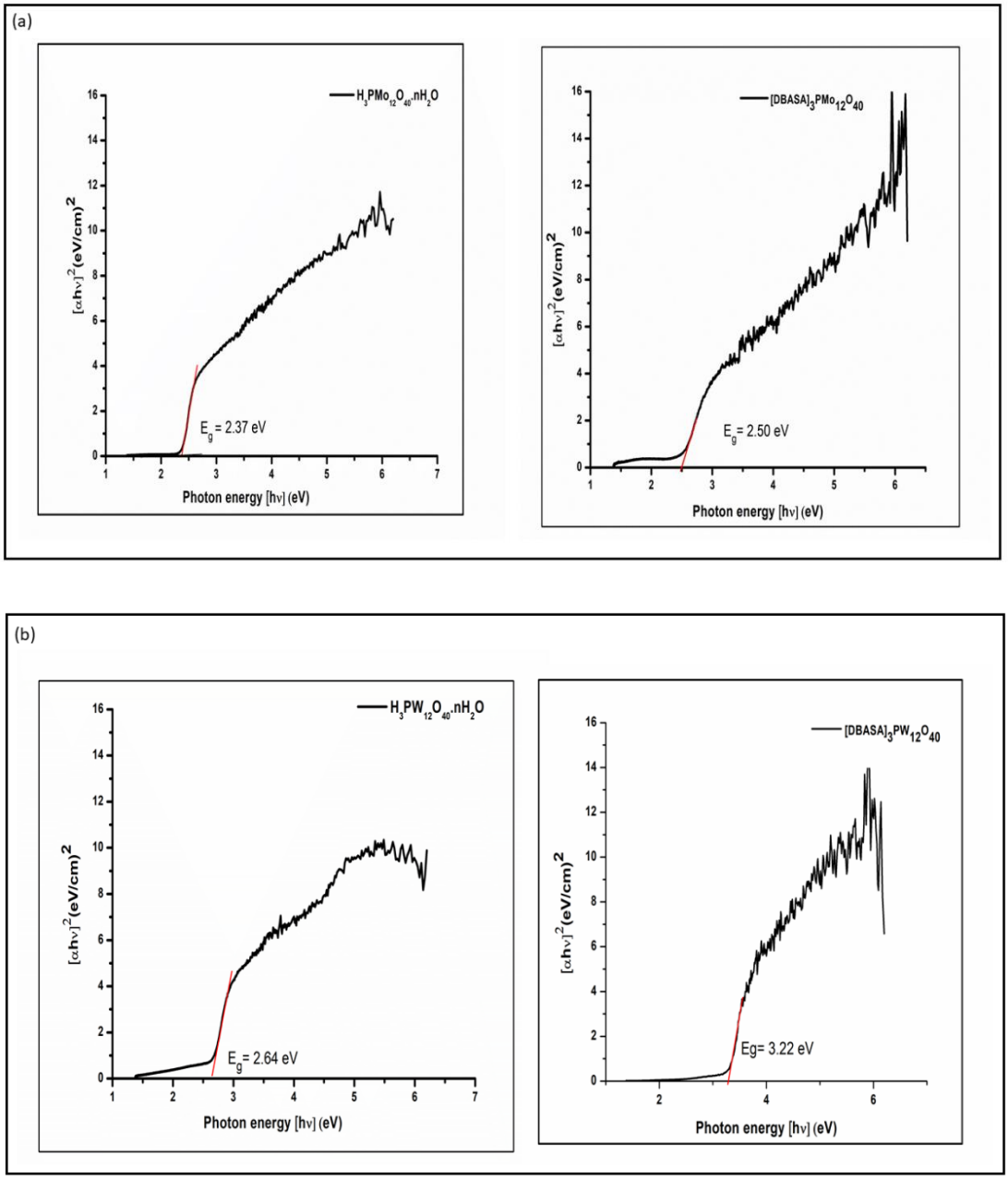

Fig. 3.9: Tauc plots of (**a**) $[DBDSA]_3[PMo_{12}O_{40}]$ and $H_3PMo_{12}O_{40}\cdot nH_2O$ (**b**) $[DBDSA]_3[PW_{12}O_{40}]$ and $H_3PW_{12}O_{40}\cdot nH_2O$.

3.2.8 SEM analysis

The SEM morphologies of the hybrid salts $[DBDSA]_3[PMo_{12}O_{40}]$ and $[DBDSA]_3[PW_{12}O_{40}]$ under similar magnification range are represented in **Fig. 3.10**. The SEM topography of phosphomolybdate hybrid in **Fig. 3.10** (**a**) reveals stacking of smaller sized agglomerates which are observed as irregular agglomeration while clustering to comparatively bigger sized structures in case of the phosphotungstate hybrid (**Fig. 3.10b**). This may be the result because of extensive secondary interactions

of intermolecular H-bonds of the two $–SO_3H$ functionality of the ammonium cation with the oxygen atoms of Keggin anions. A close view of the images also reveals thread-like structures emerging from the agglomerates. The exact reason for differences in the sizes of aggregates and the appearance of thread-looking structures is unknown and it is beyond the scope of this study. After the addition of ionic liquid to the POM, a tremendous change in the morphology has been observed. The ordered structure of the pure heteropolyacids has been converted into granular aggregated clumps.

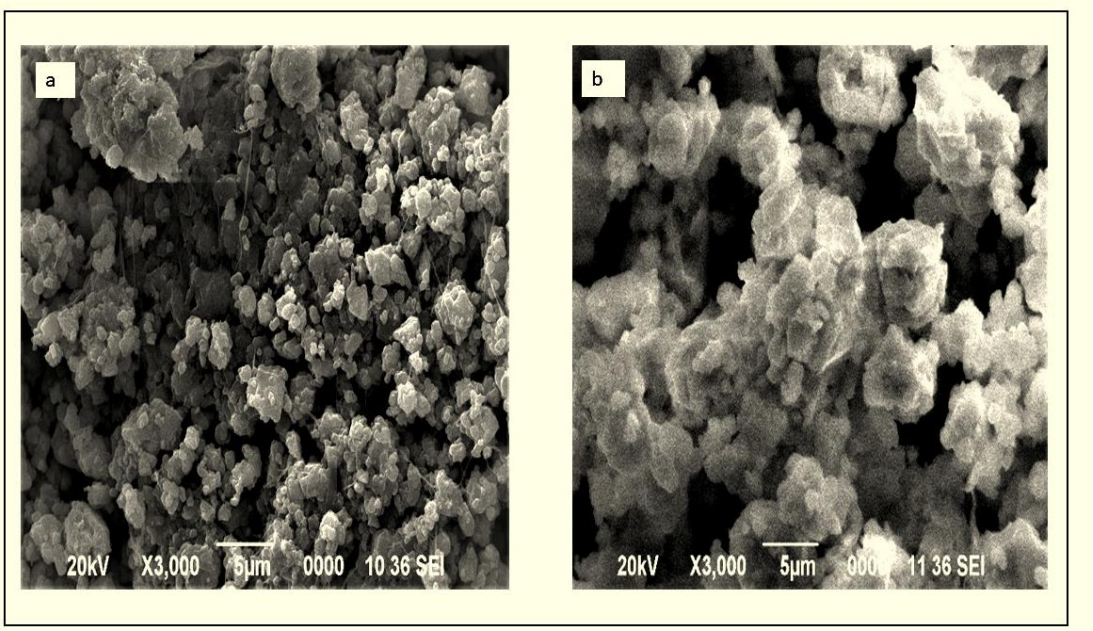

Fig. 3.10: SEM images of (**a**) $[DBDSA]_3[PMo_{12}O_{40}]$ and (**b**) $[DBDSA]_3[PW_{12}O_{40}]$.

3.2.9 EDX analysis

The EDX analysis for $[DBDSA]_3PMo_{12}O_{40}$ and $[DBDSA]_3PW_{12}O_{40}$ (**Fig. 3.11)** was carried out and all the constituent elements were detected for both the hybrids except nitrogen element**,** which is not observed in $[DBDSA]_3PMo_{12}O_{40}$. As a general rule, nitrogen may be present in low abundance compared to Mo and other elements on the surface of the Keggin anion which is why nitrogen is not detected.

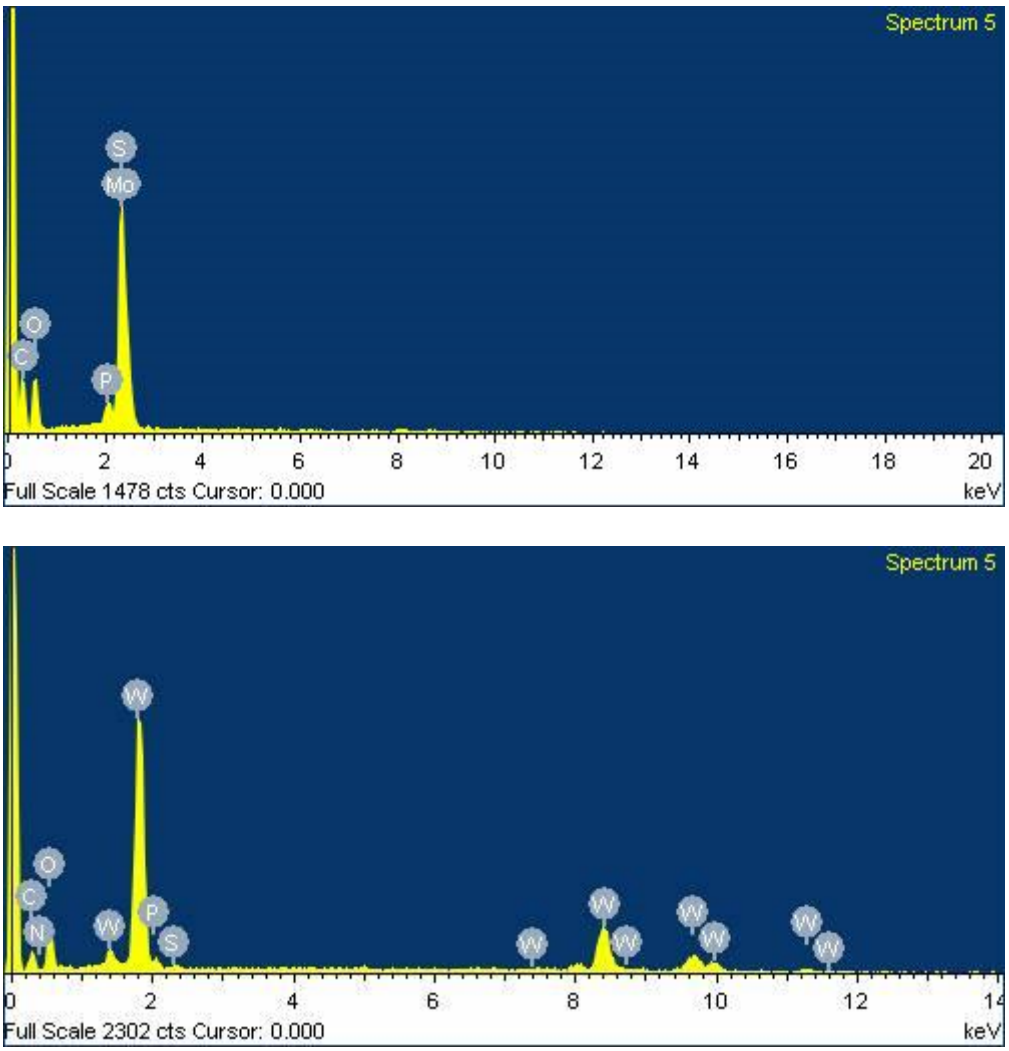

Fig. 3.11: EDX patterns of $[DBDSA]_3[PMo_{12}O_{40}]$ and $[DBDSA]_3[PW_{12}O_{40}]$.

Nevertheless, the CHN analysis proved the presence of nitrogen element and hence quantification of the nitrogen element in the hybrids is done from CHN analysis.

3.3 Catalytic activity study

3.3.1 Oxidative degradation of Metobromuron

Catalytic degradation of metobromuron in aqueous medium under sunlight in the presence of H_2O_2 (30%) was performed in a reactor using the synthesized IL-POMs i.e., $[DBDSA]_3[PMo_{12}O_{40}]$ and $[DBDSA]_3[PW_{12}O_{40}]$ as heterogeneous catalysts and the metobromuron disappearance was monitored from HPLC chromatogram [**Fig. 3.12**]. However, the mineralization of herbicide was studied by TOC removal to time. Sunlight experiments were carried out at Tezpur University, Assam, India between times 8:00 a.m. to 4:00 p.m. in the month of August. Before exposure to natural sunlight, 20 mg of the IL-POM catalyst was added into 50 mL metobromuron solution (10 mg/L) and the same

was kept at room temperature for 30 minutes in the dark to reach adsorption–desorption equilibrium. The blank solution kept in dark for 30 minutes was taken as the zero-time reading as no change in concentration was observed after 30 minutes. The reaction vessel was then placed on flat ground under sunlight with an extra addition of 0.1 mL of H_2O_2 (30%) as oxidant in presence of IL-POM catalyst. The herbicide water samples were collected from reaction vessels at regular time intervals for degradation analysis. It was observed that after 8 hours of natural solar illumination, 65% TOC removal in presence of $[DBDSA]_3PMo_{12}O_{40}$ catalyst was observed from the TOC graph plotted for 8 hours of reaction time in sub-unit 3.3.3 **[Fig. 3.16]**. However, with $[DBDSA]PW_{12}O_{40}$, we observed a TOC removal of 72% in 8 hours of illumination [**Fig. 3.16**]. Hence it was seen that both the catalysts were efficient enough to be used as oxidative degradation catalysts in sunlight in the presence of H_2O_2 (30%). Our catalyst which contains a polyoxometalate anion is said to be the activator of H_2O_2. They form a metalperoxo complex which helps in the easy transfer of oxygen for the oxidation of herbicide molecules present in water.

Although, the metobromuron disappeared from the solution in almost 8 hours, but presence of other degradation products in 8 hours may still be a matter of concern. So, we continued the reaction for another 18 hours at room temperature in absence of sunlight (natural or simulated) and monitored the TOC of further degraded solution again [**Table 3.2** & **Fig. 3.16**].

A controlled reaction was also done at room temperature with only H_2O_2 (30%) in absence of catalyst and light (natural or simulated) and kept for 8 hours. 7% of TOC removal in 8 hours was observed for metobromuron from the TOC results indicating H_2O_2 decomposes very slowly in the absence of sunlight and catalyst [**Table 3.2**].

The respective herbicide degradation experiment with $[DBDSA]_3[PW_{12}O_{40}]$ as catalyst under sunlight and without H_2O_2 was also performed. In this case, the reaction did not proceed. This observation infers that the IL-POM remains inactive without H_2O_2.

Another reaction with only H_2O_2 and without $[DBDSA]_3[PW_{12}O_{40}]$ as catalyst was performed under sunlight. It was observed that 42% of TOC removal occurs in 8 hours of sunlight.

This infers that there is an interdependency of IL-POM hybrid in activation of H_2O_2 which increases the TOC removal percentage in the presence of sunlight.

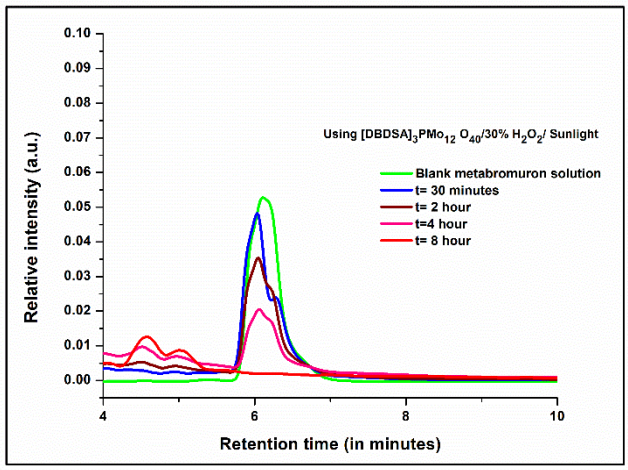

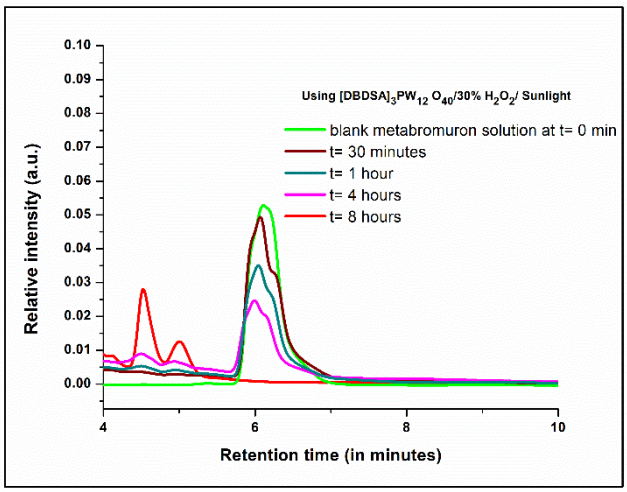

Fig. 3.12: HPLC chromatogram monitoring degradation of metobromuron with respect to time at 245 nm using 20mg of catalyst (1) $[DBDSA]_3[PMo_{12}O_{40}]$/0.1 mL 30% H_2O_2/sunlight, (2) $[DBDSA]_3[PW_{12}O_{40}]$/ 0.1 mL 30% H_2O_2/sunlight.

It was also observed from the above studies that the heterogeneous nature of the catalyst sustains throughout the reaction which is due to the presence of $-SO_3H$ functionality in the ionic-liquid cation and serves as a perfect combination for degradation of metobromuron in aqueous medium under sunlight with the addition of hydrogen peroxide. The use of dibutyldisulphoammonium $[DBDSA]^+$ cation in the precursor ionic liquid [DBDSA]Cl was preferred because introduction of the $-SO_3H$ groups to the organic cation provide intramolecular hydrogen bonding ability to the organic cation within the hybrid molecule itself. Moreover, the presence of two hydrophobic butyl groups in the ammonium unit resulted in increased hydrophobicity in the IL-POM hybrids. Thus, the anion exchange of parent chloride-based ionic liquid with the polyoxometalate anion led to extensive hydrogen bonding in the molecule as well as

with the adjacent IL-POM molecules. The choice of counter-cations of the precursor ionic liquid is important in determining the nature of the final hybrid. Although the polyoxometalate anion in the IL-POM hybrid was the active catalytic site but the heterogeneous nature of the catalyst would not have been possible with phosphotungstic acid and phosphomolybdic acid itself as these are highly soluble in water.

So, it was concluded that the reaction goes well in sunlight with synthesized IL-POM $[DBDSA]_3[PW_{12}O_{40}]$ showing slightly greater TOC removal percentage at the same time compared to $[DBDSA]_3[PMo_{12}O_{40}]$ catalyst with the addition of 0.1 mL of 30% H_2O_2 as oxidant. The TOC removal percentages of the degraded herbicide solution using $[DBDSA]_3[PW_{12}O_{40}]$ and $[DBDSA]_3[PMo_{12}O_{40}]$ are represented in **Fig. 3.16**.

3.3.2 Discussion on active species involvement with few oxidative degradation products

The HPLC chromatogram Fig. **3.12**, detects the formation of various degradation products having different retention times at different time intervals along with disappearance of metobromuron and its degradation products with time. But existence of some degradation products for a longer time may be a cause of concern for which total organic carbon (TOC) content of the herbicide solution is done further and is mentioned in the next section. After recording the data in HPLC instrument, in order to inquire about the adequate types of degradation products formed during the reaction, $[DBDSA]_3[PW_{12}O_{40}]$/0.1 mL 30% H_2O_2/sunlight at 4 hours and 8 hours respectively, the degraded metobromuron solution was collected and extracted in ethyl acetate. GC-MS was used for the identification of the degraded products of metobromuron. For this, the degraded solution was extracted with ethyl acetate (30 x 3 mL) and the organic layers were dried over Na_2SO_4, concentrated in a rotary evaporator and then GC-MS was performed for the detection of oxidative products. There was no evidence of presence of metobromuron in the degraded solution after 8 hours of reaction although formations of several other oxidative degradation products were observed both at an interval of 4 hours and 8 hours. Thus, the characteristic reactions encountered in the reaction**,** $[DBDSA]_3[PW_{12}O_{40}]$/0.1 mL 30% H_2O_2/sunlight are (a) hydroxylation of aromatic compounds (b) H-abstraction (c) dehalogenation (d) decarboxylation (e) demethylation/ demethoxylation etc. Similarly, the herbicide solution stirred for next 18 hours of

reaction time at room temperature in absence of sunlight was also subjected to GC-MS for product analysis.

During investigation of the metobromuron degradation in $[DBDSA]_3[PW_{12}O_{40}]$/0.1 mL 30% H_2O_2/sunlight (4 hours), the formation of intermediates and their plausible degradation pathways depending on the intermediates identified through analysis are depicted in Scheme 2, 3, 4 and 5 (**Fig. 3.13**). The structures of new intermediates were identified by their molecular ion (M^+) and their mass fragment ions in the GC-MS spectra. Product 1 exhibited molecular ion peak, m/z =229/227 (**Fig. 3.14**, **spectrum 1**) indicating the replacement of OCH_3 by H. The main fragment patterns are m/z= 197, 169, 91, 77 and the mechanism of fragmentation of demethoxylated product, 1-(4-bromophenyl)-3-methylurea is described in (**Fig. 3.13**, **Scheme 2**). The formation of product 1 and its fragmentation can be supported by (**Fig. 3.13**, **Scheme 5** and **Scheme 2**), and one of its fragment ions is observed as molecular ion (**Fig. 3.14, spectrum 2**), depicting simultaneous formation of various products at the same time and breaking of those products into different smaller products. Formation of product 2 is 3-(-4 hydroxyphenyl)-1 methoxy-1-methylurea is explained *via* (**Fig. 3.13, Scheme 3**). Product 2 is the dehalogenated as well as hydroxylated product with molecular ion m/z= 197 with fragment ions at m/z= 165, 135, 105. The presence of hydroxylated product in the degraded solution infers the involvement of OH• radical in the degradation mechanism. It is possible that product 2 is being attacked by Br• forming intermediate with molecular weight=135 g/mol, which might have been attacked by OH• radical forming product 3 i.e. bromo(4-hydroxyphenyl)carbamic acid, with molecular ion m/z= 230 with fragment ions at m/z= 185, 109 is justified from (**Fig. 3.14, Spectrum 4**) which may undergo further degradation into smaller molecules *via* **Fig. 3.13, Scheme 4**. Product 5, is 1-bromo-4-isocyanatobenzene (**Fig. 3.14, Spectrum 2**) with molecular ion m/z= 199/197 with main fragment patterns m/z=171/169, 90, 63. Product 4 with molecular ion m/z=173/171 with main fragment m/z= 92, 65 corresponds to 4-bromo aniline (**Fig. 3.14, Spectrum 5**). Formation of product 4 and 5 can be observed *via* **Fig. 3.13, Scheme 5**. Interestingly, the degraded solution collected after 8 hours of reaction time was observed to still contain only product 4 and 5 prominently with product 5 as the major one (**Fig. 3.15, spectrum 6 and 7**). The herbicide solution analysed after 26 hours of reaction in which the 1st 8 hours were under sunlight and the next 18 hours in absence of sunlight, didn't contain any of the products, we observed earlier in the 1st 4 and 8 hours of reaction time. Although many products in very small quantities might have not

been detected or identified due to the unavailability of adequate analysis techniques. These results indicate that the reaction was still going on at room temperature in absence of sunlight which resulted in disappearance of products from the solution. Product 5, 1-bromo-4-isocyanatobenzene which appeared to be the major product after 8 hours of reaction can be converted into various unsymmetrical disubstituted urea derivatives on addition of amines in water which transforms product 5 into a value-added product. Reports on one-pot reaction of substituted isocyanates with amines for synthesis of unsymmetrical disubstituted urea in aqueous medium in absence of catalyst were published by Mane et al. [41].

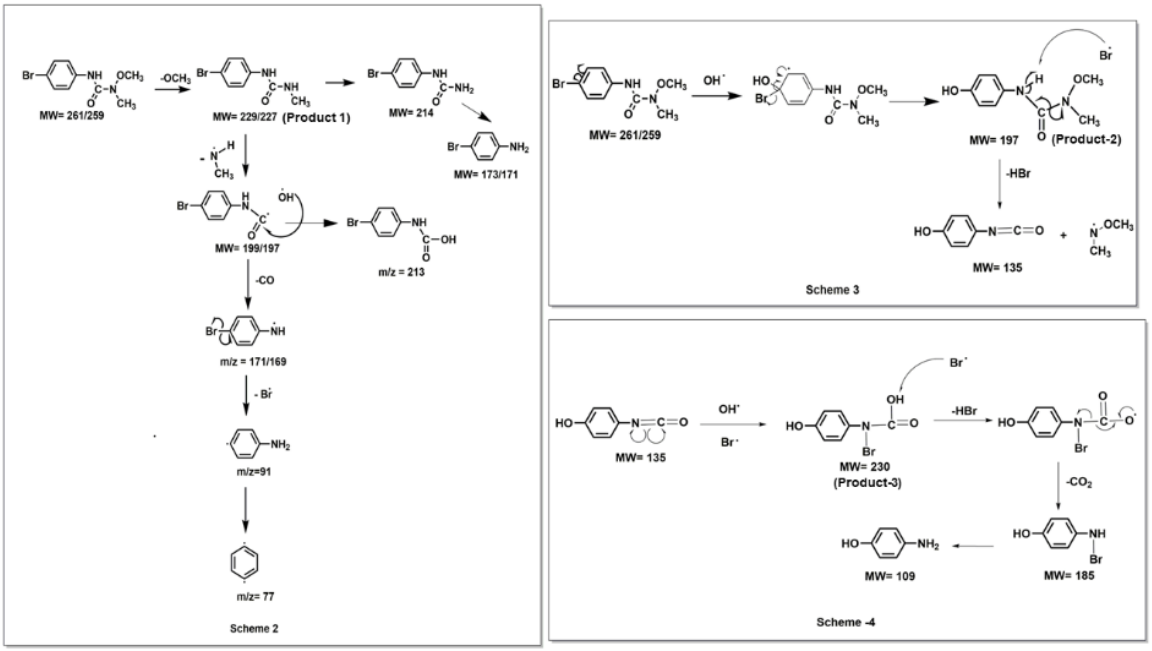

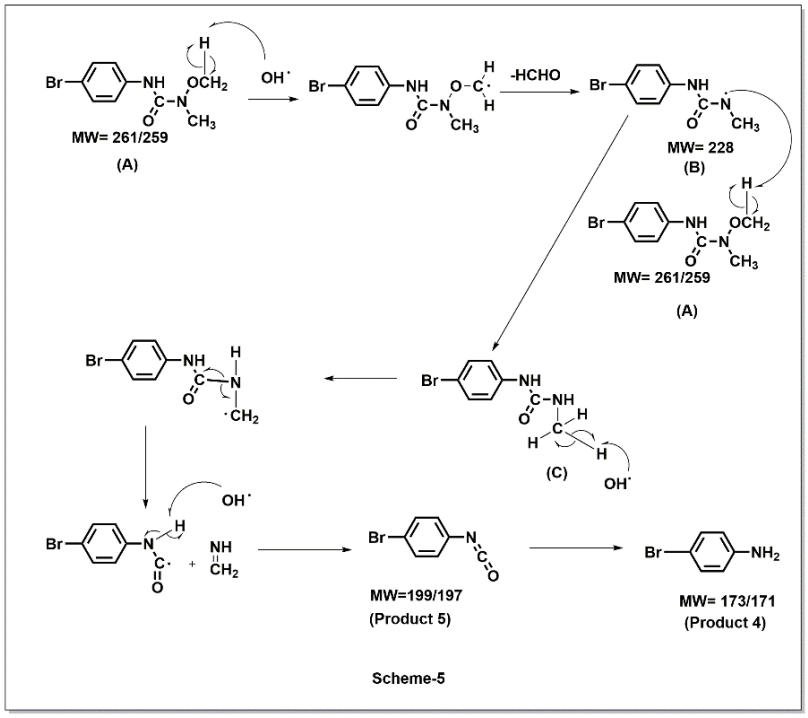

Fig. 3.13: Schemes of mechanism for the formation of different degradation products of metobromuron using $[DBDSA]_3[PW_{12}O_{40}]$/0.1 mL 30% H_2O_2/sunlight.

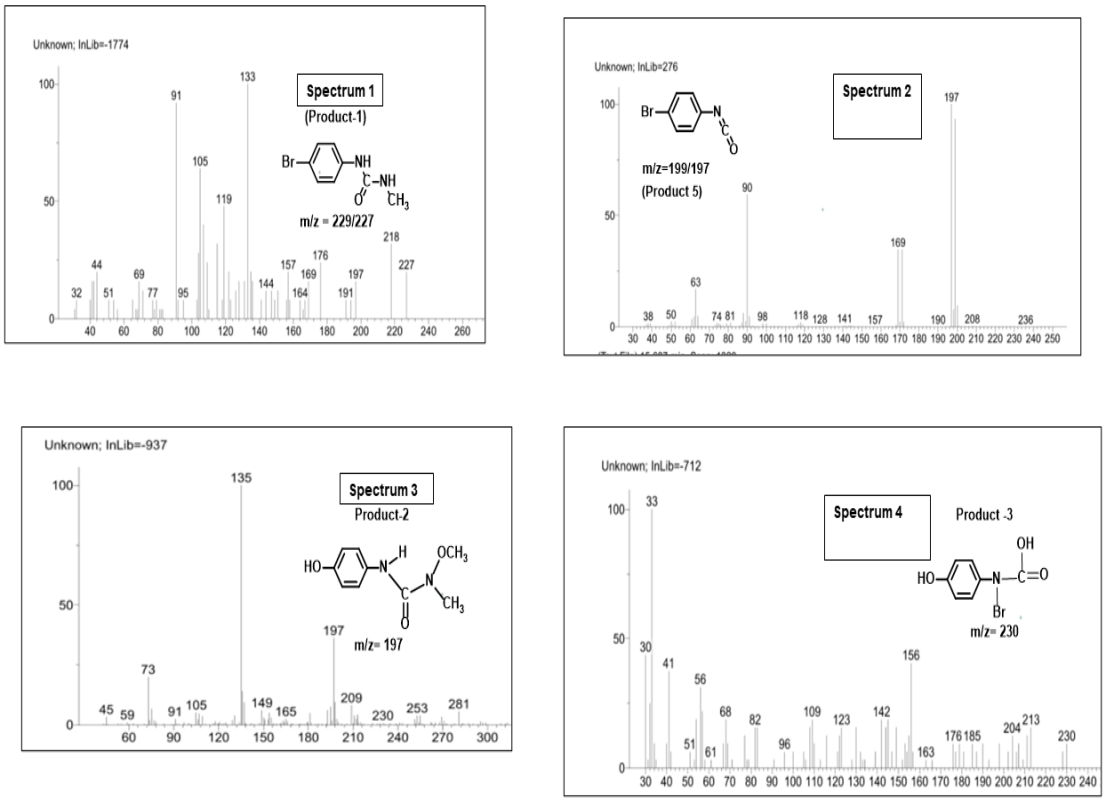

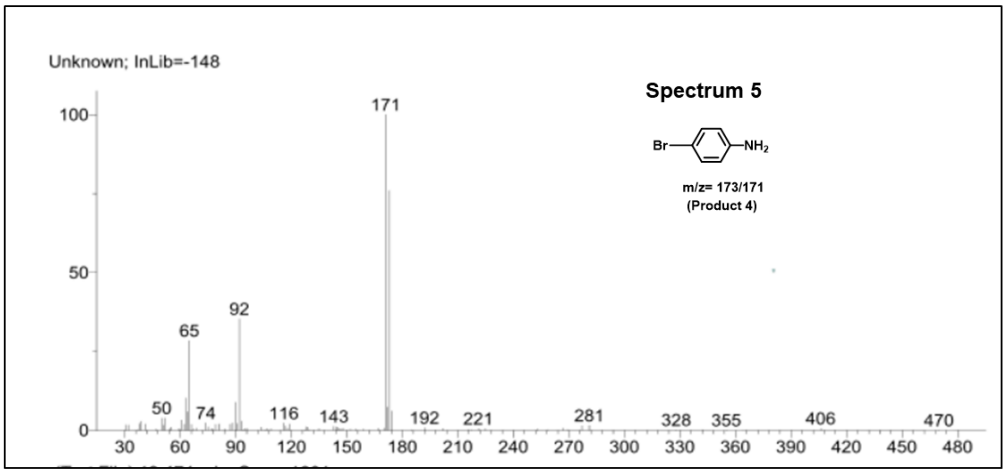

Fig. 3.14: Mass spectra of degradation products (1, 2, 3, 4, 5) observed using $[DBDSA]_3[PW_{12}O_{40}]$/0.1 mL 30% H_2O_2/sunlight (4 hour).

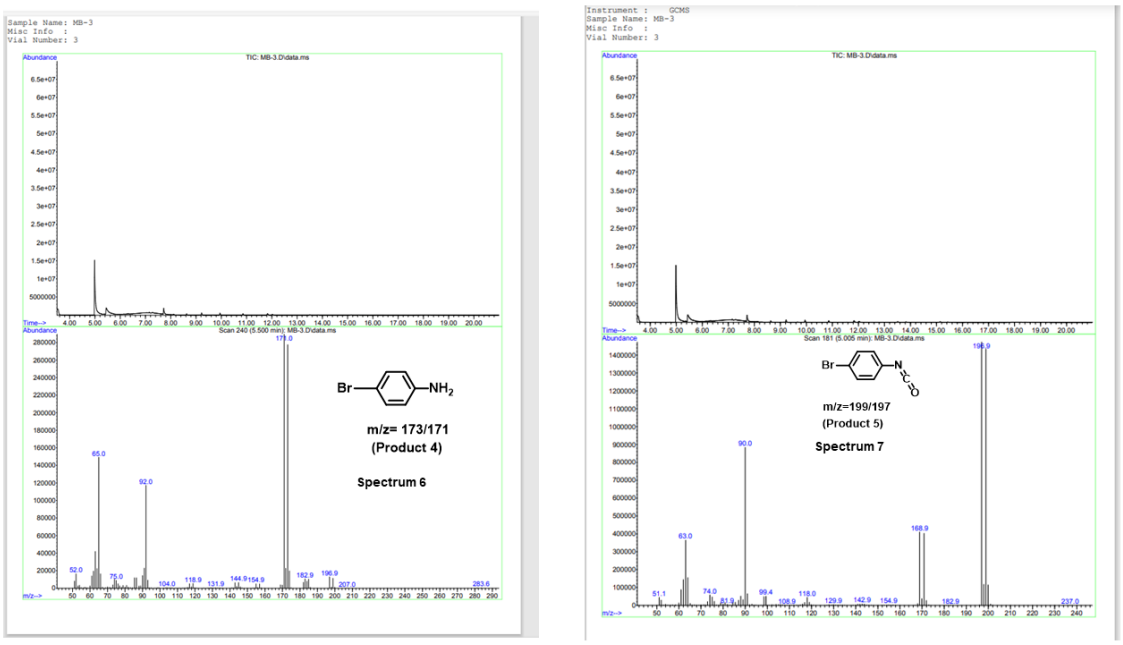

IL Mass spectra of degradation products observed using $[DBDSA]_3[PW_{12}O_{40}]$/0.1 mL 30% H_2O_2/sunlight (8 hour).

3.3.3 TOC determination:

From the products studied above in $[DBDSA]_3[PW_{12}O_{40}]$/0.1 mL 30% H_2O_2/sunlight (8 hours) we noticed that although metobromuron disappeared after almost 8 hours of continuous reaction in sunlight, degraded products formed by transformation of aromatic ring were still observed till long reaction hours, which may further be degraded into CO_2

and H_2O and other inorganic ions. Thus, disappearance of metobromuron does not indicate the decrease in toxicity as the products formed may be more toxic. So, we extend our studies towards checking the TOC for another 18 hours without sunlight (**Fig. 3.16**). To study the extent of the mineralization process, we measured the TOC as non-purgeable organic (NPOC) content of the herbicide solution at the beginning of the reaction and then at an interval of 1, 2, 4, 6, 8, 26 hours in which the 1st 8 hours of reaction is subjected to sunlight and in next 18 hours, the reaction is kept in room-temperature in stirring without sunlight. It was observed that within 8 hours of reaction time, the NPOC value decreased from 12.64 ppm to 3.576 ppm using $[DBDSA]_3[PW_{12}O_{40}]$/0.1 mL 30% H_2O_2/sunlight (8 hours) and 4.451 ppm using $[DBDSA]_3[PMo_{12}O_{40}]$/0.1 mL 30% H_2O_2/sunlight (8 hours). It can be seen, that there is progressive decrease in NPOC value from 3.576 ppm to 2.54 ppm within next 18 hours of reaction time and no further decrease in TOC was observed after that. The percentage of TOC removal using $[DBDSA]_3[PW_{12}O_{40}]$/0.1 mL 30% H_2O_2/sunlight reached 80% in 26 hours. In case of $[DBDSA]_3[PMo_{12}O_{40}]$/0.1 mL 30% H_2O_2/sunlight, the TOC removal reached 68.4% in 26 hours. The NPOC data are tabulated in **Table 3.2**. The decrease in NPOC value even at room temperature in absence of sunlight for next 18 hours infers that the catalyst can react with H_2O_2 even in absence of sunlight. It can be concluded in presence of sunlight and IL-POM catalyst, the hydrogen peroxide decomposition is faster. However, the decomposition was still occurring in the absence of sunlight as observed from TOC results. The NPOC data infers that the rate has decreased in the absence of sunlight.

Table 3.2: NPOC value of the degraded metobromuron solution at different time intervals in various experimental condition

Entry	Initial NPOC value (ppm)	Time (In hours)	NPOC value after (degradation using $[DBDSA]_3PW_{12}O_{40}$ / 30% H_2O_2/ sunlight	NPOC value after (degradation using $[DBDSA]_3PMo_{12}O_{40}$ / 30% H_2O_2/ sunlight	NPOC value after (degradation using 30% H_2O_2 in room temperature and $[DBDSA]_3PW_{12}O_{40}$ in dark)	NPOC value after (degradation using 30% H_2O_2 in sunlight)
1.	12.64	1	9.396	9.774	-	-
2.	12.64	2	6.698	7.216	-	-
3.	12.64	4	5.881	6.450	-	-

4.	12.64	6	4.896	5.010	-	-
5.	12.64	8	3.576	4.450	11.73	7.4
6.	12.64	26	2.54[a]	3.991[a]	-	-

[a] The time given 26 hours in this table is the NPOC value is of the next 18 hours after the herbicide solution was taken away from 8 hours of sunlight exposure.

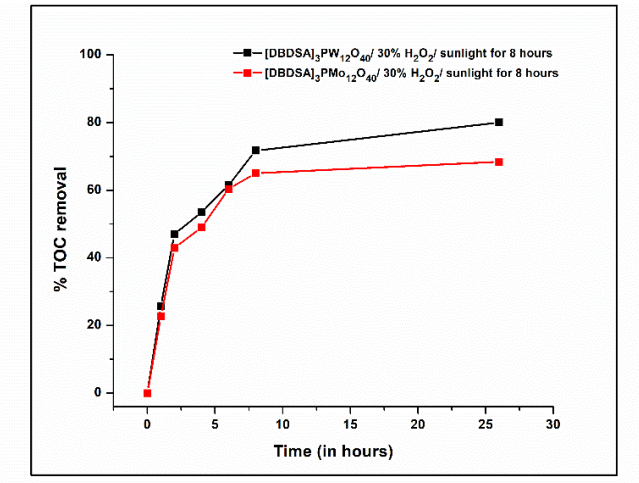

Fig. 3.16: Comparative % TOC removal plots of metobromuron using (**a**) $[DBDSA]_3[PMo_{12}O_{40}]$/0.1 mL 30% H_2O_2/sunlight (8 hours) and next 18 hours in absence of sunlight, (**b**) $[DBDSA]_3[PW_{12}O_{40}]$/ 0.1 mL 30% H_2O_2/sunlight (8 hours) and next 18 hours in absence of sunlight.

Table 3.3: Comparison table of the catalyst $[DBDSA]_3PW_{12}O_{40}$ with various reported techniques for degradation of metobromuron

Entry	Techniques/ Degradation results	Reference
1.	**TiO_2 photocatalysts/90% mineralization**	**42**
2.	**Laccase by fermentation (Biosolid based crude enzyme extract)/Negligible activity towards metobromuron**	**43**
3.	**Photo-Fenton pre-treatment followed by a biological system with immobilized biomass/ not compatible for complete mineralization of metobromuron**	**44**
4.	**$[DBDSA]_3PW_{12}O_{40}$, H_2O_2, Sunlight/ 72% TOC removal**	**Current work**

A comparison table has been provided in **Table 3.3** that compares the activity of the present catalyst with other reported catalysts. Apart from the techniques mentioned in **Table 3.3,** no literature is found for removal of the metobromuron with other techniques like adsorption and membrane separation which need secondary pollution treatment. Using the oxidative degradation process [IL-POM/H_2O_2/sunlight], the pollutant

undergoes degradation into smaller products and mineralizes into CO_2 and water. The degradation products found at certain time intervals can be used as value-added substrates for various important organic reactions which was observed in the present work. Moreover, the catalyst recovery and recyclability are very easy in the case of heterogeneous catalytic system.

3.4 Plausible mechanism of generation of active species via IL-POM in degradation process

Discussing the mechanism using IL-POM catalyst/ 0.1 mL 30% H_2O_2/sunlight, the IL-POM hybrid, catalyst upon encountering the H_2O_2 forms an active peroxide intermediate *via* transfer of oxygen from H_2O_2, **Scheme 3.2**. The strong interaction *via* intermolecular hydrogen bonding of the -SO_3H group with the POM anion enhances the degradation efficiency. The involvement of OH• radicals can be justified by the detection of hydroxylated products during degradation formed as a result of the reaction of hydroxyl radicals with substrate resulting in product no 2 (**Fig. 3.14, Spectrum 3**). The generation of metal-peroxo intermediate in the reaction process is justified from the FT-IR spectroscopy of the used catalyst isolated in the middle of the reaction process as solid residue (**Fig. 3.17**). It was observed that two new peaks at 630 cm^{-1} and 506 cm^{-1} are assigned to the symmetric and asymmetric stretching vibration of terminally η2-coordinated O_2^{2-} ligand to W [45, 46]. This also evidenced that the catalyst was retained as heterogeneous phase during the catalytic reaction as the used catalyst showed presence of active metal peroxo intermediate which was formed after the addition of H_2O_2.

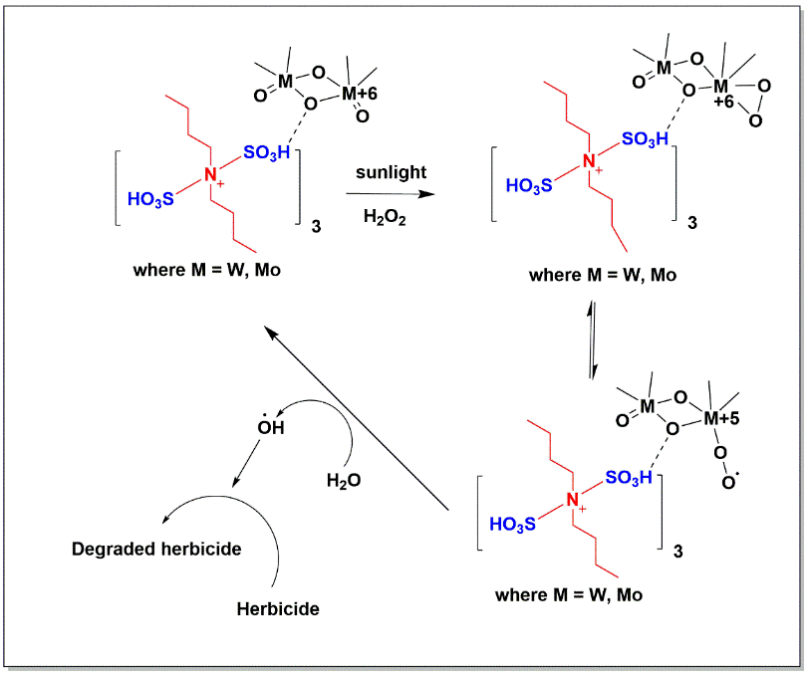

Scheme 3.2: Mechanism of degradation using IL-POM catalyst in IL-POM/ 30% H_2O_2/sunlight.

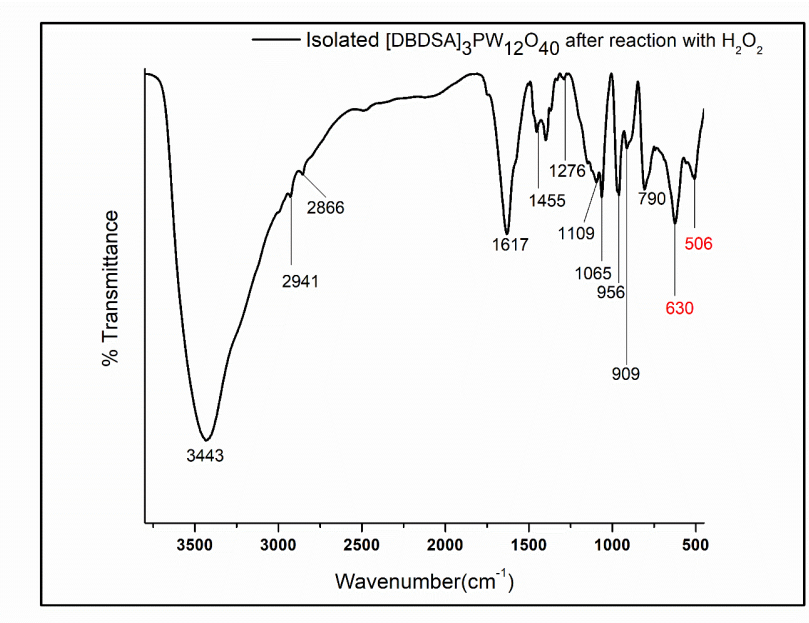

Fig. 3.17: FT-IR spectrum of isolated catalyst in experiment $[DBDSA]_3[PW_{12}O_{40}]$/0.1 mL 30% H_2O_2/sunlight

3.5 Recyclability study of the catalyst

The reusability of catalyst was assessed only for 20 mg of catalyst $[DBDSA]_3[PW_{12}O_{40}]$/ Sunlight/ 0.1 mL 30%H_2O_2 up to 8 hours and next the reaction continued for 18 hours at room temperature in absence of light. The recycled catalyst $[DBDSA]_3[PW_{12}O_{40}]$ showed up to > 70% degradation of metobromuron even after three consecutive uses as evidenced from TOC study (**Fig. 3.18**). The negligible loss of catalytic activity of reused catalyst after each cycle can be reasoned efficient active metal-peroxo complex formation of catalyst and remarkable stability of the metal peroxo species. Recovery of the catalyst was done by centrifugation of the degraded solution; the catalyst settled down the centrifuge tube and then washed properly with water and dichloromethane to remove inorganic and organic impurities, respectively. The PXRD of the used catalyst showed visible differences compared to the fresh one, implying that the catalyst changes into other forms with addition of H_2O_2. However, most of the characteristic peaks retained its position same as the fresh catalyst in **Fig. 3.19**.

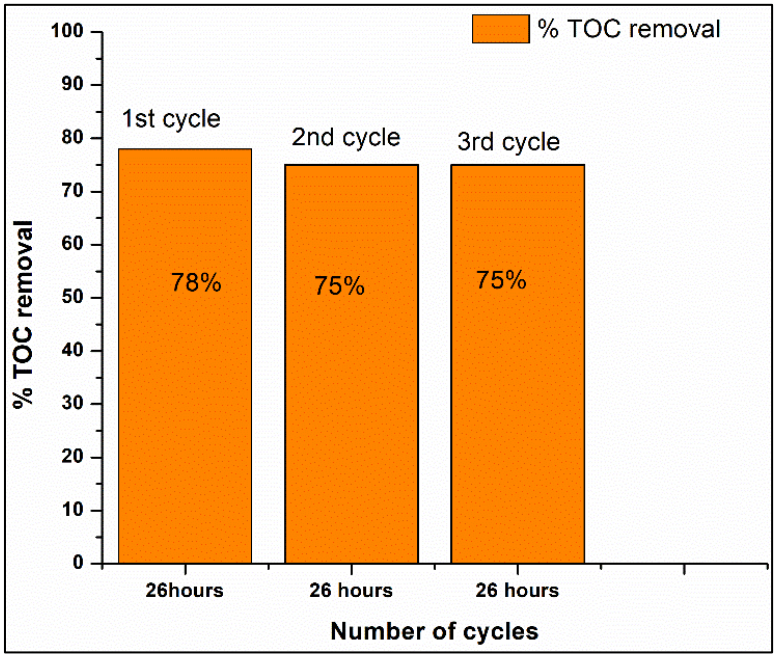

Fig. 3.18: Recyclability study based on TOC removal % using $[DBDSA]_3[PW_{12}O_{40}]$ for 3 consecutive cycles.

To have a clear understanding of the structure of the $[DBDSA]_3[PW_{12}O_{40}]$ after addition of H_2O_2, the ^{31}P NMR of spent $[DBDSA]_3[PW_{12}O_{40}]$ catalyst after 3 consecutive cycles was analysed and represented in **Fig. 3.20**. From, the NMR spectrum, it can be said that a new peak arises at -0.99 ppm for the spent $[DBDSA]_3[PW_{12}O_{40}]$ apart from the single peak observed for fresh $[DBDSA]_3[PW_{12}O_{40}]$. However, the intensity of -15.04 ppm is much higher compared to the newly appeared peak in the **Fig. 3.20**. This indicates that

only a small part of the $[PW_{12}O_{40}]^{3-}$ might have been converted into other forms. Since on addition of the H_2O_2 on $[DBDSA]_3[PW_{12}O_{40}]$, there is the possibility of generation of metal peroxo complex as observed in FTIR spectrum (**Fig. 3.17**), however, the new peak at -0.99 ppm **(Fig. 3.20)** shows formation of fully or partially peroxidized species leading to Venturello anion ($PW_4O_{24}^{3-}$) from literature [47].

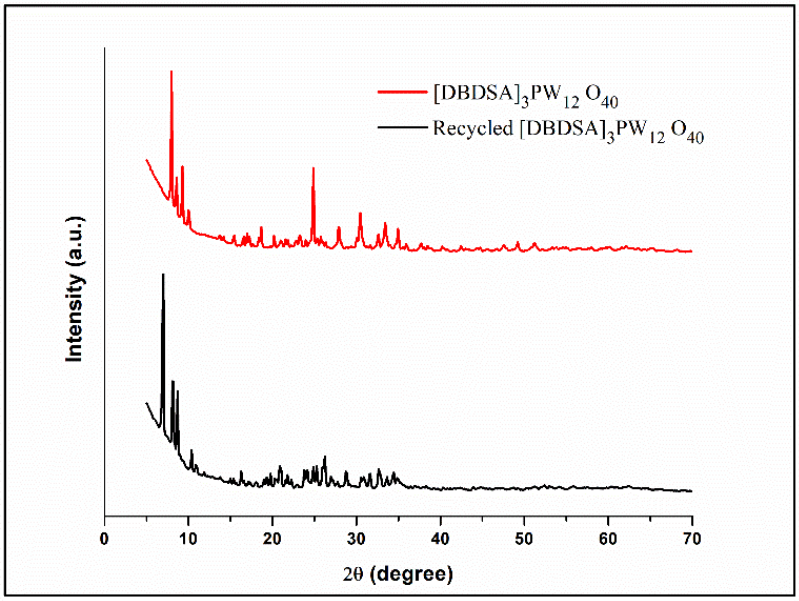

Fig. 3.19: PXRD of the used catalyst $[DBDSA]_3[PW_{12}O_{40}]$ after 3 consecutive reaction cycles.

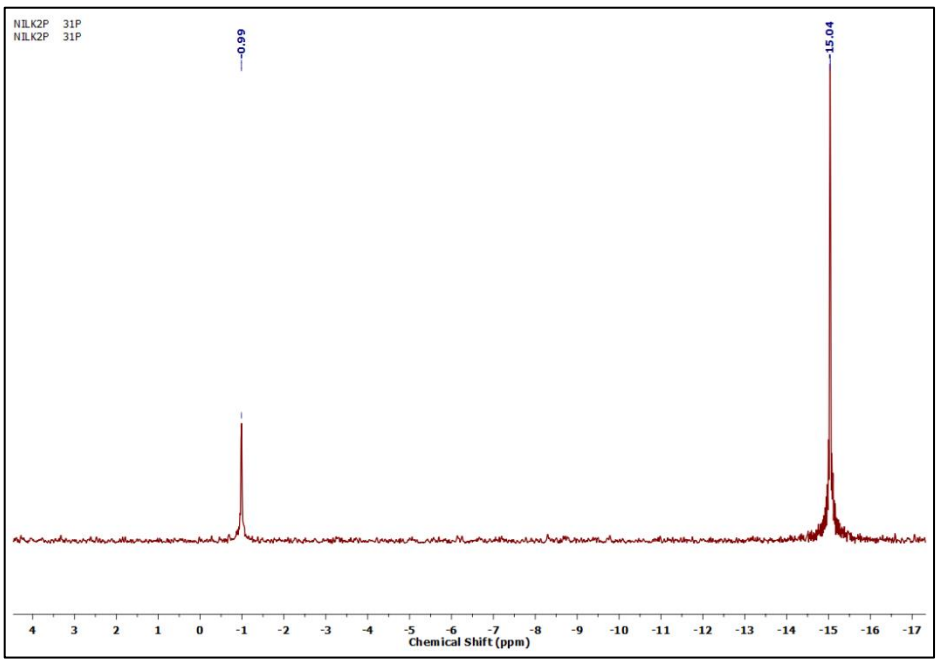

Fig. 3.20: ^{31}P NMR of spent $[DBDSA]_3[PW_{12}O_{40}]$ after 3 consecutive reaction cycles.

3.6 Heterogeneity of the catalyst

Heterogeneity of the catalysts was confirmed using UV-Visible spectroscopy as no peak of the catalyst was observed after 26 hours of reaction time after filtration of catalyst, (Fig 3.21).

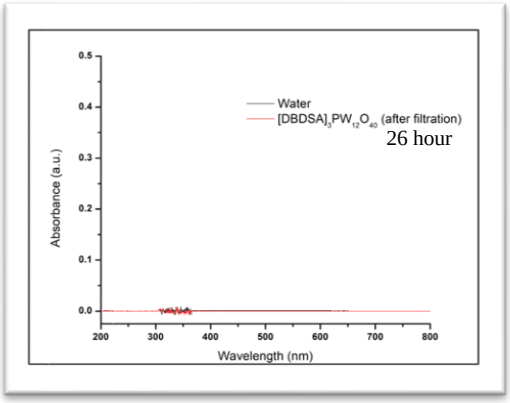

Fig. 3.21: UV-Visible spectra of the reaction solution after catalyst filtration after 26 hours of reaction time.

3.7 Conclusions

In summary, two N-SO_3H functionalized water-insoluble heterogeneous IL-POM catalysts, $[DBDSA]_3[PMo_{12}O_{40}]$ and $[DBDSA]_3[PW_{12}O_{40}]$ were synthesized. Both served as efficient oxidative degradation catalysts for degradation of metobromuron when used with H_2O_2 as an oxidant in the presence of sunlight This research may supply new insight into the usage of functionalized IL and POM-based catalysis materials as this method was cost-effective and encourages us to further develop functionalized heterogeneous IL-POM systems, in which heterogeneity is preserved throughout the reaction.

The novelty of designing the respective IL-POMs, $[DBDSA]_3[PMo_{12}O_{40}]$ and $[DBDSA]_3[PW_{12}O_{40}]$ lies in the fact that these are insoluble in nature which would not have been possible with the parent phosphotungstic acid and phosphomolybdic acid itself as these are highly soluble in water. Although the polyoxometalate anion in the IL-POM hybrids was the active catalytic site, the heterogeneous nature of the catalyst which persisted throughout the reaction was because of the structure of the counter-cation with -SO_3H functionalization that resulted in intramolecular H-bonding along with ion-dipole interactions within cation and anion of the molecules. The presence of two butyl groups

in the ammonium core cationic structure also resulted in the generation of water-insoluble nature in the IL-POMs.

The reaction resulted in 1-bromo-4-isocyanatobenzene as the major value-added product which can be used as one of the substrates for synthesis of various unsymmetrical disubstituted urea derivatives. The efficiency of these catalysts, both in the presence and absence of sunlight was proved by the results obtained from TOC removal data. The strong electrostatic interactions, hydrogen bonds within $-SO_3H$ functional group and POM anion are the main driving forces for the structural stability of the hybrid materials and retention of heterogeneity throughout the reaction. The ability to design and incorporate functional groups into parent ionic liquid cation that serves the purpose specific to the need of the task provides great potential in the usage of these functionalized IL-POM hybrids as oxidative catalysts in the presence of H_2O_2 as oxidant. This method proves to be an eco-friendly approach in degradation studies of phenylurea herbicide in aqueous medium.

3.8 Experimental Section

3.8.1 Preparation of dibutyldisulfoammonium salts of Keggin anion $[DBDSA]_3PM_{12}O_{40}$ where M= Mo & W

The polyoxometalate hybrid salt $[DBDSA]_3PM_{12}O_{40}$ of dibutyl disulfoammonium cation $[DBDSA]^+$ containing phosphomolybdate anion/phosphotungstate anion $[PM_{12}O_{40}]^{3-}$, M= Mo and W were prepared in two steps (**Scheme 3.1**). The 1st step involved for preparation of dibutyl disulfoamonium chloride ionic liquid [DBDSA]Cl through the dropwise addition of chlorosulfonic acid (20 mmol) into a stirring solution of dibutylamine in dry hexane (10 mL) in a round bottom flask at 0 ºC for 10 minutes till the evolution of HCl gas. Then the reaction mixture was allowed to stir for 1 hour to obtain chloride ionic liquid [DBDSA]Cl as a separate layer in hexane for the next step of reaction. Dry hexane (3 × 10 mL) was used repeatedly to wash soluble impurities from the crude [DBDSA]Cl layer by decantation. After that, the chloride IL was dried in a vacuum oven at 50 ºC to obtain the purest form of straw-colored ionic liquid.

In second step the synthesized $[DBDSA]Cl{\cdot}nH_2O$ was mixed with $H_3PMo_{12}O_{40}{\cdot}nH_2O$ (PMA) or $H_3PW_{12}O_{40}{\cdot}nH_2O$ (PTA) in 3:1 ratio to produce the $[DBDSA]_3PM_{12}O_{40}$ hybrid salts. For this purpose, 1 mmol of $H_3PM_{12}O_{40}{\cdot}nH_2O$, M= Mo, W was stirred in 20 mL of

distilled water at room temperature and then 3 mmol of [DBDSA]Cl·nH_2O was added dropwise to the aqueous solution of $H_3PMo_{12}O_{40}$·nH_2O. Instant yellow precipitation was observed after the addition of [DBDSA]Cl·nH_2O. Similarly, the addition of [DBDSA]Cl to aqueous solution of $H_3PW_{12}O_{40}$·nH_2O led to formation of a white precipitate insoluble in water. Both the reaction mixtures were allowed to stir for 12 hours to get maximum yields. After that, the reaction mixtures were centrifuged to get the solid product. The isolated respective solids were dried in a vacuum oven at 80 ºC for 12 hours to get analytically pure IL-POM hybrids.

3.8.2 Procedure for metobromuron degradation

20 mg of $[DBDSA]_3PW_{12}O_{40}$ and $[DBDSA]_3PMo_{12}O_{40}$ were used separately for 50 mL metobromuron solution (10 mg/L) and were kept at 2 different vessels at room temperature for 30 minutes in dark to reach adsorption–desorption equilibrium. The degradation of metobromuron in both vessels was then conducted under natural sunlight in atmospheric conditions during daytime in the presence of 0.1 mL of H_2O_2 (30%). From each of the reaction vessels, 0.25 mL sample solution were collected at different time intervals and then analyzed by HPLC instrument. The reaction was performed under natural sunlight for 8 hours and then kept at room temperature for the next 18 hours. The reaction progress was monitored by HPLC, and it helps in detection of the appearance of any new degradation products with time along with disappearance of metobromuron. GC–MS was used for identification of the degraded products of metobromuron that formed during the oxidative degradation process. For both the reactions, the degraded solutions of metobromuron were collected as filtrate after separation of the catalyst as solid residue and then washed with added (3 mL) water for recycling. Then the degradation products of metobromuron were extracted from the filtrate with ethyl acetate (30 × 3 mL) and dried over anhydrous sodium sulfate. The ethyl acetate solution was concentrated in rotary evaporator and GC-MS analysis was performed to detect the products collected over certain time intervals. The total organic carbon (TOC) content of the degraded metobromuron solution over time was plotted for percentage TOC removal during the reaction using the data collected from the TOC instrument.

3.9 Spectral data

Table 3.4: Spectral data of the parent ionic liquid and ionic liquid-polyoxometalate hybrids

Structure	**Spectral data**
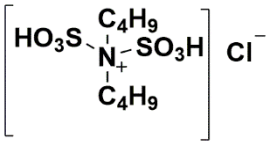 [DBDSA]Cl	Light brown liquid; FT-IR(KBr) υcm^{-1} = 3448, 2960, 2935, 2866, 1628, 1455, 1229, 1168, 1053, 1016, 873, 847, 583; ^{1}HNMR (DMSO-d_6, 400MHz): δ 8.47 (s, 2H), 2.75(t, 4H, 12Hz), 1.49(quintet, 4H J= 8Hz), 1.17-1.26 (sextet, J= 8 Hz, 4H), 0.78 (t, *J*= 8Hz, 6H); ^{13}CNMR (DMSO-d_6, 100MHz): δ 13.70, 19.70, 27.66, 47.10; CHN analysis: Calculated for [DBDSA]Cl (%): C 29.49, H 6.19, N 4.30 Found: C 29.0, H 6.10, N 4.52.
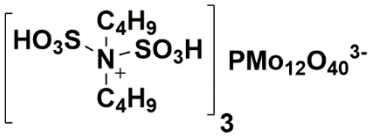 [DBDSA]$_3$[PMo$_{12}$O$_{40}$]	Yellow amorphous solid; FT-IR(KBr) υcm^{-1} =3588, 3484, 3192, 3070, 2960, 2935, 2869, 1595, 1455, 1377, 1229, 1165, 1065, 956, 870, 790, 583; ^{1}HNMR (DMSO-d_6, 400MHz): δ 8.15 (s, 2H), 2.84(t, 4H, 16Hz), 1.50(quintet, 4H, J= 8Hz), 1.24-1.34 (sextet, J= 8 Hz, 4H), 0.86 (t, *J*= 8Hz, 6H); ^{13}CNMR (DMSO-d_6, 100MHz): δ 14.01, 19.77, 28.09, 47.09; ^{31}P NMR (DMSO-d_6, 202 MHz): δ -3.50. CHN analysis: [DBDSA]$_3$PMo$_{12}$O$_{40}$ (%): C 10.60, H 2.20, N 1.54, Found: C 11.01, H 2.15, N 1.56.
	White amorphous solid; FT-IR(KBr) υcm^{-1} = 3491, 3100, 2960, 2935, 2866, 1595,

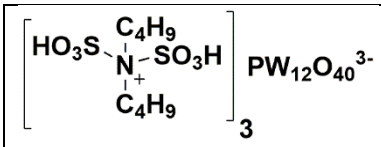 [DBDSA]$_3$[$PW_{12}O_{40}$]	1455, 1165, 1229, 1065, 956, 870, 790, 583; ^{1}HNMR (DMSO-d_6, 400MHz): δ 8.11 (s, 2H), 2.84(t, 4H, 16Hz), 1.50(quintet, 4H, J= 8Hz), 1.24-1.34 (sextet, J= 8 Hz, 4H), 0.86 (t, J= 8Hz, 6H); ^{13}CNMR (DMSO-d_6, 100MHz): δ 14.02, 19.77, 28.09, 47.07; ^{31}P NMR (DMSO- d_6, 202 MHz): δ -15.0. [DBDSA]$_3PW_{12}O_{40}$ (%): C 7.68, H 1.60 N 1.12. Found: C 7.92, H 1.67, N 1.08.

3.10 Bibliography

[1] Faust, S. D., and Aly, O. M. Water pollution by organic pesticides. *Journal-American Water Works Association*, 56(3): 267-279, 1964.

[2] Tom Lin, C. *The Pesticide Manual*, British Crop Protection Council, Inc., Farnham, 2000.

[3] Hoda, N., Bayram, E., and Ayranci, E. Removal of metobromuron pesticide from aqueous solutions by adsorption at high area activated carbon cloth. *Innovations in Chemical Biology*, 225-232, 2009.

[4] Navarro, S., Hernandez-Bastida, J., Cazana, G., Perez-Lucas, G., and Fenoll, J. Assessment of the leaching potential of 12 substituted phenyl urea herbicides in two agricultural soils under laboratory conditions. *Journal of Agricultural and Food Chemistry*, 60(21): 5279-5286, 2012.

[5] Hao, X., Chen, Q., van Loosdrecht, M. C., Li, J., and Jiang, H. Sustainable disposal of excess sludge: Incineration without anaerobic digestion. *Water Research*, 170: 115298, 2020.

[6] Simpson, D. R. Biofilm processes in biologically active carbon water purification. *Water Research*, 42(12): 2839-2848, 2008.

[7] Kutzer, S., Wintrich, H., and Mersmann, A. Air stripping–a method for treatment of wastewater. *Chemical Engineering & Technology: Industrial Chemistry-Plant Equipment-Process Engineering-Biotechnology*, 18(3): 149-155, 1995.

[8] Andreozzi, R., Caprio, V., Insola, A., and Marotta, R. Advanced oxidation processes (AOP) for water purification and recovery. *Catalysis Today*, 53(1): 51-59, 1999.

[9] Chiron, S., Fernandez-Alba, A., and Rodriguez, A. Garcia--Calvo E. Pesticide chemical oxidation: state of the art. *Water Res*, 34(2): 366-377, 2000.

[10] Chong, M. N., Jin, B., Chow, C. W., and Saint, C. Recent developments in photocatalytic water treatment technology: A review. *Water Research*, 44(10): 2997-3027, 2010.

[11] Devipriya, S. and Yesodharan, S. Photocatalytic degradation of pesticide contaminants in water. *Solar Energy Materials and Solar Cells*, 86(3): 309-348, 2005.

[12] Herrmann, J. M. Heterogeneous photocatalysis: Fundamentals and applications to the removal of various types of aqueous pollutants. *Catalysis Today*, 53(1): 115-129, 1999.

[13] Hoffmann, M. R., Martin, S. T., Choi, W., and Bahnemann, D. W. Environmental applications of semiconductor photocatalysis. *Chemical Reviews*, 95(1): 69-96, 1995.

[14] Malato, S., Blanco, J., Cáceres, J., Fernández-Alba, A. R., Agüera, A., and Rodrıguez, A. Photocatalytic treatment of water-soluble pesticides by photo-Fenton and TiO_2 using solar energy. *Catalysis Today*, 76(2-4): 209-220, 2002.

[15] Gkika, E., Kormali, P., Antonaraki, S., Dimoticali, D., Papaconstantinou, E., and Hiskia, A. Polyoxometallates as effective photocatalysts in water purification from pesticides. *International Journal of Photoenergy*, 6: 227-231, 2004.

[16] Mylonas, A., Hiskia, A., and Papaconstantinou, E. Contribution to water purification using polyoxometalates. Aromatic derivatives, chloroacetic acids. *Journal of Molecular Catalysis A: Chemical*, 114(1-3):191-200, 1996.

[17] Hiskia, A., Troupis, A., and Papaconstantinou, E. Environmental photocatalytic processes with POM. The photodecomposition of atrazine and photoreduction of metal ions from aqueous solutions. *International Journal of Photoenergy*, 4: 35-40, 2002.

[18] Hiskla, A., Androulaki, E., Mylonas, A., Troupis, A., and Papaconstantinou, E. Photocatalytic Decontamination by Polyoxometalates. In Pope, M. T., Müller, A., editors, *Polyoxometalate Chemistry from Topology via Self-Assembly to Applications*, Springer, Dordrecht, 2001.

[19] Van Rompuy, L. S. and Parac-Vogt, T. N. Interactions between polyoxometalates and biological systems: From drug design to artificial enzymes. *Current Opinion in Biotechnology*, 58: 92-99, 2019.

[20] Velessiotis, D., Douvas, A. M., Athanasiou, S., Nilsson, B., Petersson, G., Södervall, U., Alestig, G., Argitis, P., and Glezos, N. Molecular junctions made of tungsten-polyoxometalate self-assembled monolayers: Towards polyoxometalate-based molecular electronics devices. *Microelectronic Engineering*, 88(8): 2775-2777, 2011.

[21] Dehghani, R., Aber, S., and Mahdizadeh, F. Polyoxometalates and their composites as photocatalysts for organic pollutants degradation in aqueous media—a review. *CLEAN–Soil, Air, Water*, 46(12):1800413, 2018.

[22] Mylonas, A. and Papaconstantinou, E. Photocatalytic degradation of chlorophenols to CO_2 and HCl with polyoxotungstates in aqueous solution. *Journal of Molecular Catalysis*, 92(3): 261-267, 1994.

[23] Mylonas, A. and Papaconstantinou, E. On the mechanism of photocatalytic degradation of chlorinated phenols to CO_2 and HCl by polyoxometalates. *Journal of Photochemistry and Photobiology A: Chemistry*, 94(1): 77-82, 1996.

[24] Suzuki, K., Mizuno, N., and Yamaguchi, K. Polyoxometalate photocatalysis for liquid-phase selective organic functional group transformations. *ACS Catalysis*, 8(11): 10809-10825, 2018.

[25] Gaya, U. I. and Abdullah, A. H. Heterogeneous photocatalytic degradation of organic contaminants over titanium dioxide: a review of fundamentals, progress and problems. *Journal of Photochemistry and Photobiology C: Photochemistry Reviews*, 9(1): 1-12, 2008.

[26] Konstantinou, I. K. and Albanis, T. A. Photocatalytic transformation of pesticides in aqueous titanium dioxide suspensions using artificial and solar light: intermediates and degradation pathways. *Applied Catalysis B: Environmental*, 42(4): 319-335, 2003.

[27] Guo, Y. and Hu, C. Heterogeneous photocatalysis by solid polyoxometalates. *Journal of Molecular Catalysis A: Chemical*, 262(1-2): 136-148, 2007.

[28] Guo, Y., Wang, Y., Hu, C., Wang, Y., Wang, E., Zhou, Y., and Feng, S. Microporous polyoxometalates POMs/SiO_2: Synthesis and photocatalytic degradation of aqueous organocholorine pesticides. *Chemistry of Materials*, 12(11): 3501-3508, 2000.

[29] Lei, P., Chen, C., Yang, J., Ma, W., Zhao, J., and Zang, L. Degradation of dye pollutants by immobilized polyoxometalate with H_2O_2 under visible-light irradiation. *Environmental Science & Technology*, 39(21): 8466-8474, 2005.

[30] Li, H., Gao, S., Cao, M., and Cao, R. Self-assembly of polyoxometalate–thionine multilayer films on magnetic microspheres as photocatalyst for methyl orange degradation under visible light irradiation. *Journal of Colloid and Interface Science*, 394: 434-440, 2013.

[31] Ivanova, S. Hybrid organic-inorganic materials based on polyoxometalates and ionic liquids and their application in catalysis. *International Scholarly Research Notices*, 2014, 2014.

[32] Ren, Y., Wang, M., Chen, X., Yue, B., and He, H. Heterogeneous catalysis of polyoxometalate based organic–inorganic hybrids. *Materials*, 8(4): 1545-1567, 2015.

[33] Bridgeman, A. J. Density functional study of the vibrational frequencies of α-Keggin heteropoly anions. *Chemical Physics*, 287(1-2): 55-69, 2003.

[34] Rao, G. R. and Rajkumar, T. Interaction of Keggin anions of 12-tungstophosphoric acid with $Ce_xZr_{1-x}O_2$ solid solutions. *Journal of Colloid and Interface Science*, 324(1-2): 134-141, 2008.

[35] Ganapathy, S., Fournier, M., Paul, J. F., Delevoye, L., Guelton, M., and Amoureux, J. P. Location of protons in anhydrous Keggin heteropolyacids $H_3PMo_{12}O_{40}$ and $H_3PW_{12}O_{40}$ by ^1H $\{^{31}P\}/^{31}P$ $\{^1H\}$ REDOR NMR and DFT quantum chemical calculations. *Journal of the American Chemical Society*, 124(26): 7821-7828, 2002.

[36] Gong, Y., Guo, Y., Hu, Q., Wang, C., Zang, L., and Yu, L. pH-responsive polyoxometalate-based supramolecular hybrid nanomaterials and application as renewable catalyst for dyes. *ACS Sustainable Chemistry & Engineering*, 5(5): 3650-3658, 2017.

[37] Bridgeman, A. J. Computational atudy of the vibrational spectra of α-and β-Keggin polyoxometalates. *Chemistry–A European Journal*, 10(12): 2935-2941, 2004.

[38] Sasca, V. and Popa, A. Band-gap energy of heteropoly compounds containing Keggin polyanion-$[PV_xMo_{12-x}O_{40}]^{-(3+x)}$ relates to counter-cations and temperature studied by UV-VIS diffuse reflectance spectroscopy. *Journal of Applied Physics*, 114(13): 133503, 2013.

[39] Jubu, P. R., Yam, F. K., Igba, V. M., and Beh, K. P. Tauc-plot scale and extrapolation effect on bandgap estimation from UV–vis–NIR data–a case study of β-Ga_2O_3. *Journal of Solid-State Chemistry*, 290: 121576, 2020.

[40] Khan, M. I. and Swenson, L. S. New and Future Developments in Catalysis, Hybrid Materials, Composites, and Organocatalysts. Elsevier, Amsterdam, 2013.

[41] Mane, M., Balaskar, R., Gavade, S., Pabrekar, P., and Mane, D. An efficient and greener protocol towards synthesis of unsymmetrical N, N′-biphenyl urea. *Arabian Journal of Chemistry*, 6(4): 423-427, 2013.

[42] Amine-Khodja, A., Boulkamh, A., and Richard, C. Photo transformation of metobromuron in the presence of TiO_2. *Applied Catalysis B: Environmental*, 59(3-4): 147-154, 2005.

[43] Vaithyanathan, V. K., Vaidyanathan, V. K., and Cabana, H. Laccase-driven transformation of high priority pesticides without redox mediators: Towards bioremediation of contaminated wastewaters. *Frontiers in Bioengineering and Biotechnology*, *9*: 770435, 2022.

[44] Parra, S., Sarria, V., Malato, S., Péringer, P., and Pulgarin, C. Photochemical versus coupled photochemical–biological flow system for the treatment of two biorecalcitrant herbicides: Metobromuron and isoproturon. *Applied Catalysis B: Environmental*, 27(3): 153-168, 2000.

[45] Das, N., Chowdhury, S., and Purkayastha, R. N. D. Peroxo–tungstate (VI) complexes: syntheses, characterization, reactivity, and DFT studies. *Monatshefte für Chemie-Chemical Monthly*, 150: 1255-1266, 2019.

[46] Dengel, A. C., Griffith, W. P., Powell, R. D., and Skapski, A. C. Studies on transition-metal peroxo complexes. Part 7. Molybdenum (VI) and tungsten (VI) carboxylato peroxo complexes, and the X-ray crystal structure of $K_2[MoO(O_2)_2(glyc)]\cdot 2H_2O$. *Journal of the Chemical Society, Dalton Transactions*, (5): 991-995, 1987.

[47] de La Garza L. C, Vigier, K. D. O., Chatel G., and Moores, A. Amphiphilic dipyridinium-phosphotungstate as an efficient and recyclable catalyst for triphasic fatty ester epoxidation and oxidative cleavage with hydrogen peroxide. *Green Chemistry*, 19: 2855-2862, 2017.